Review

Bo Fu*, Jingxuan Sun, Gang Wang, Ce Shang, Yuxuan Ma, Jianguo Ma, Lijun Xu and Vittorio Scardaci*

Solution-processed two-dimensional materials for ultrafast fiber lasers (invited)

https://doi.org/10.1515/nanoph-2019-0558
Received December 28, 2019; revised February 3, 2020; accepted February 4, 2020

Abstract: Since graphene was first reported as a saturable absorber to achieve ultrafast pulses in fiber lasers, many other two-dimensional (2D) materials, such as topological insulators, transition metal dichalcogenides, black phosphorus, and MXenes, have been widely investigated in fiber lasers due to their broadband operation, ultrafast recovery time, and controllable modulation depth. Recently, solution-processing methods for the fabrication of 2D materials have attracted considerable interest due to their advantages of low cost, easy fabrication, and scalability. Here, we review the various solution-processed methods for the preparation of different 2D materials. Then, the applications and performance of solution-processing-based 2D materials in fiber lasers are discussed. Finally, a perspective of the solution-processed methods and 2D material-based saturable absorbers are presented.

***Corresponding authors: Bo Fu,** BUAA-CCMU Advanced Innovation Center for Big Data-Based Precision Medicine, Interdisciplinary Innovation Institute of Medicine and Engineering, Beihang University, Beijing 100191, P.R. China; and School of Instrumentation and Optoelectronic Engineering, Beihang University, Beijing 100191, P.R. China, e-mail: fubo10@buaa.edu.cn. https://orcid.org/0000-0003-1409-2666; and **Vittorio Scardaci,** Dipartimento di Scienze Chimiche, Universitá degli Studi di Catania, Catania, Italy, e-mail: vittorio.scardaci@unict.it. https://orcid.org/0000-0003-0167-4368
Jingxuan Sun, Gang Wang and Yuxuan Ma: School of Instrumentation and Optoelectronic Engineering, Beihang University, Beijing 100191, P.R. China
Ce Shang: BUAA-CCMU Advanced Innovation Center for Big Data-Based Precision Medicine, Interdisciplinary Innovation Institute of Medicine and Engineering, Beihang University, Beijing 100191, P.R. China; and School of Biological Science and Medical Engineering, Beihang University, Beijing 100191, P.R. China
Jianguo Ma and Lijun Xu: BUAA-CCMU Advanced Innovation Center for Big Data-Based Precision Medicine, Interdisciplinary Innovation Institute of Medicine and Engineering, Beihang University, Beijing 100191, P.R. China; and School of Instrumentation and Optoelectronic Engineering, Beihang University, Beijing 100191, P.R. China

Keywords: solution-processed; 2D materials; fiber laser; pulse.

1 Introduction

Lasers able to generate pulses on a picosecond time scale or less have widespread applications in science and technology [1]. Among these, fiber lasers have advantages such as alignment-free operation, efficient heat dissipation, and compact designs, making them particularly attractive for applications requiring a stable operation [2, 3]. For example, in medicine, stable pulses operating at ~2 μm are required for surgery due to the water absorption at this wavelength [4, 5], while pulses operating in the ~1–1.5 μm range are required for imaging, to minimize photodamage and maximize penetration depth [6]. Owing to their high performance, design flexibility, and low maintenance costs [7, 8], fiber lasers have been particularly successful in applications such as medicine [9, 10], telecommunication [11], and sensing [12]. Optical pulses, as required by most applications, are generated by a mode-locking or Q-switching technique [13, 14], where an intensity-dependent saturable absorber (SA) is typically used [15]. SAs with high modulation depths (e.g. 41.2% and 51.3% [16, 17]) and low saturation intensity (e.g. 0.75 and 2.02 MW/cm^2 [18, 19]) are typically desired for mode locking of fiber lasers due to their higher gain and lower cavity losses compared with solid-state lasers [20]. To date, the most common SAs used in commercial fiber lasers are based on semiconductor SA mirrors (SESAMs) [21] and non-linear polarization evolution [22]. However, SESAMs generally have a limited bandwidth (~100 nm [21]), while non-linear polarization evolution-based SAs are sensitive to environmental parameters [22], resulting in stringent technological requirements needed to control their properties. These limitations are particularly detrimental for scientific research and technological development. For example, from a laser design perspective, SAs able to provide flexible parameters (e.g. low linear absorption

and high modulation depth), and that can be easy to fabricate and integrate, are especially desirable [23, 24]. These requirements, driven by a growing number of scientific and industrial applications, motivate research on new materials, novel designs, and technologies [25–28].

Two-dimensional materials (2DMs) have emerged as promising SAs with a number of favorable properties for laser development [29, 30], such as broadband operation [31, 32], controllable modulation depth [33], and ultrafast recovery time [34, 35]. In addition, they can be solution processed by means of wet chemistry [36], making them easy to fabricate and integrate into all-fiber configurations. Since the first demonstration of a graphene SA produced by liquid-phase exfoliation (LPE) [37], a growing number of related 2DMs are being investigated due to their diverse properties and manufacturing flexibility [30]. Among these, SAs based on topological insulators (TIs) have been demonstrated with high (~95%) modulation depth [38], while transition metal dichalcogenides (TMDs) have better saturable absorption response (1.38 MW/cm^2 [39]) compared with graphene (e.g. 60 and 266 MW/cm^2 [40, 41]). Moreover, black phosphorus (BP) with a large span of bandgap and controllable band energy (0.3 eV for bulk BP and 2 eV for monolayer BP) that can be controlled by the number of layers has also proved to be a broadband SA up to the mid-infrared band [42].

Here, we review recent developments toward the implementation of solution-processed 2DMs to fiber lasers and present our outlook on this field. The exfoliation, stabilization, sorting, and MXene fabrication are discussed in Section 2. Then, the applications of solution-processed 2DM-based ultrafast fiber lasers are presented. Finally, a summary and outlook is given in Section 4.

2 Fabrication methods

The two main methods to produce 2DMs (i.e. crystalline materials with a layered structure) can be categorized into bottom-up and top-down [43]. For example, chemical vapor deposition (CVD) is a popular bottom-up method able to produce high-quality, large-area materials [44–46]. While CVD is used for applications such as integrated electronic devices [47, 48] or transparent electrodes, for other applications such as solar cells, fuel cells, thermoelectric devices, or optical sensing systems [49–52], it is preferable to have the 2DMs dispersed in a liquid, which would make them easier to process and manipulate [53, 54].

LPE of 2DMs is a typical top-down method where a bulk crystal or powder (of the starting material) is exfoliated in a liquid medium by disrupting the forces keeping the layers together [43]. It can be achieved by using physical forces (e.g. ultrasound waves or shear forces [53, 55, 56]) or by chemically modifying the layers, e.g. by intercalation (e.g. insertion of ions or use of electrochemical actions [56]), or by oxidation [57, 58]. Compared to CVD, which requires high substrate temperatures followed by transfer to the target substrate, LPE has the advantages of scalability, room temperature processing, and high yield, and does not require any substrate [43]. Dispersions produced by LPE can be easily integrated into various systems like batteries or solar cells [49]. Here, we provide a brief overview of the main LPE methods used to achieve stable 2DM dispersions for ultrafast laser applications.

LPE is one of the most popular methods to produce 2DM-based SAs. From the SA perspective, a number of aspects need to be considered when evaluating an LPE method. For example, the yield of single or few layers, as well as their concentration, is important to maximize the modulation depth [59], while the dispersion stability (i.e. the ability to prevent reaggregation [53]) is crucial as aggregates could cause non-saturable scattering losses [60]. Other aspects such as cost and scalability are clearly important from a technology implementation standpoint [53, 61]. Regardless of the type of forces involved, there are three main steps in achieving stable dispersions: actual exfoliation, stabilization, and sorting. Herein, we summarize the typical LPE-based 2DM SAs, as shown in Table 1.

2.1 Exfoliation methods

Exfoliation is the process by which the layered structure of a 2DM is disrupted to form individual layers or few-layer structures [133–135]. The most popular exfoliation method used to fabricate SAs is ultrasonication, in which ultrasound waves are employed to disrupt the weak inter-layer van der Waals forces within the 2D crystal (Figure 1A, B). Ultrasonication has proved effective for most 2DM-based SAs, including graphene [36, 41, 62–67, 133], TIs [16, 59, 89, 91, 105, 107–111, 114, 136–138], TMDs [19, 39, 60, 74, 83–89, 91, 92, 96, 97, 99–104, 135, 139–142], and BP [42, 116–130, 143–145]. Its popularity arises from the ease of use, low cost, and immediate availability across most laboratories [55, 146, 147]. Conversely, scalability is an issue for such methods, as ultrasonication remains essentially a laboratory-based process [55].

Intercalation is another popular method used to exfoliate 2DMs for SA preparation. The intercalation process can occur by using intercalants (typically small ions like Li^+) or by electrochemistry [56]. The process relies on the

Table 1: Summary of the typical LPE-based 2DM SAs.

Material	Exfoliation	Medium/stabilization	Integration	Ref.
Graphene	Ultrasonication	PVA	PVA composite	[62]
Graphene	Ultrasonication	Surfactant	PVA composite	[36, 41, 63–66]
Graphene	Ultrasonication	Surfactant or solvent (NMP or ODCB)	PVA or SMMA composite	[61]
Graphene	Ultrasonication	NMP	SMMA composite	[67]
Graphene	Electrochemistry	Sulfuric acid	Photonic crystal fiber	[68]
GO	Acid treatment	–	PPV composite	[69]
GO	Hummers	–	Optical deposition	[40]
GO	Hummers	–	PVA composite	[70–72]
GO	–	–	Photonic crystal fiber	[73]
GO	–	–	Spray	[74–76]
RGO	Hummers/hydrazine	–	Self-assembled membrane	[77]
RGO	Hummers/hydrazine	–	Optical deposition	[78–81]
GO and RGO	Hummers/benzylamine	–	Deposited on fused silica	[82]
MoS_2	Ultrasonication	Surfactant	PVA composite	[19, 83, 84]
MoS_2	Ultrasonication	DMF	PVA composite	[85–88]
MoS_2	Ultrasonication	IPA	PVA composite	[89]
MoS_2	Intercalation	Li-ion and ethylene glycol	Optical deposition	[90]
WS_2	Ultrasonication	Surfactant	PVA composite	[39, 84, 91, 92]
WS_2	Ultrasonication	NMP	PVA composite	[88]
WS_2	Intercalation	Hydrazine and Na-ion	Optical deposition on tapered fiber	[93]
WS_2	Intercalation	Li-ion in ethanol	Spin coating on side polished fiber	[94]
WS_2	Intercalation	Li-ion and butyl-lithium in hexane	PVA composite	[95]
$WS_2/MoSe_2$	Ultrasonication	Surfactant	PVA composite	[96]
WS_2	Ultrasonication	Water and ethanol	Optical deposition or PVA composite	[97]
$MoSe_2$	Ultrasonication	Surfactant	PVA composite	[60, 84]
$MoSe_2$	Intercalation	Hydrazine and Na-ion	Optical deposition	[98]
WSe_2	Ultrasonication	Surfactant	PVA composite	[84, 99]
TiS_2	Ultrasonication	NMP	Optical deposition	[100]
SnS_2	Ultrasonication	Alcohol	PVA composite	[101, 102]
ReS_2	Ultrasonication	NMP	PVA composite	[103]
$PtTe_2$	Ultrasonication	IPA	PVA composite	[104]
Bi_2Te_3	Ultrasonication	Surfactant	PVA composite	[91]
Bi_2Te_3	Ultrasonication	NMP	PVA composite	[105]
Bi_2Te_3	Intercalation	Li-ion and ethylene glycol	Drop cast on CaF_2 lens	[17]
Bi_2Te_3	Intercalation	Li-ion and ethylene glycol	Solution-filled photonic crystal fiber	[106]
Bi_2Se_3	Ultrasonication	NMP	Optical deposition	[59]
Bi_2Se_3	Ultrasonication	NMP	PVA composite	[105, 107–109]
Bi_2Se_3	Ultrasonication	IPA	Drop-cast on quartz plate	[110]
Bi_2Se_3	Ultrasonication	IPA	Transfer onto fiber end facet	[111]
Bi_2Se_3	Intercalation	Li-ion and ethylene glycol	Optical deposition	[112, 113]
Bi_2Te_3	Ultrasonication	NMP	Solution-filled photonic crystal fiber	[114]
Sb_2Te_3	Stirring	Water and chitosan	Drop-cast on side-polished fiber	[115]
BP	Ultrasonication	IPA	Optical deposition	[116–118]
BP	Ultrasonication	NMP	Optical deposition	[119–124]
BP	Ultrasonication	NMP	PVA composite	[125–128]
BP	Ultrasonication	NMP	Deposited on Au mirror	[116, 117]
BP	Ultrasonication	NMP	Inkjet printing	[129]
BP	Ultrasonication	Surfactant	PVA composite	[130]
BP	Electrochemistry	Tetra-*n*-butyl-ammonium bisulfate	Transfer onto fiber adapter	[131]
BP	Electrochemistry	Tetra-*n*-butyl-ammonium bisulfate	Sandwiched freestanding film	[132]

PVA, polyvinyl alcohol; SMMA, styrene methylmethacrylate; NMP, *N*-methyl-2-pyrrolidone; ODCB, ortho-dichlorobenzene; PPV, polyphenylene vinylene; DMF, dimethyl formamide; IPA, isopropyl alcohol.

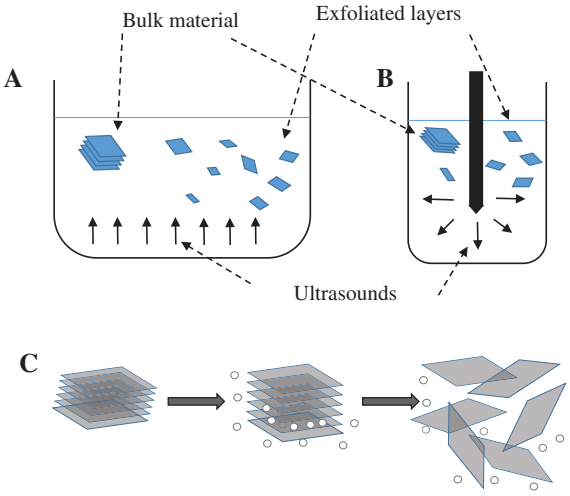

Figure 1: Schematics of the main exfoliation methods.
(A) Bath ultrasonication. (B) Tip ultrasonication. (C) Intercalation.

insertion of an ion or a molecule into a 2DM structure to disrupt its inter-layer forces (Figure 1C). For SA fabrication, intercalating ions have been used for TMDs [90, 93–95] and TIs [17, 38, 106, 112, 113, 148–155]. Lithium ions (Li^+) were first used to produce MoS_2 monolayers using a chemical reaction with *n*-butyl lithium [156]. In this case, such reaction produced molecular hydrogen (H_2), which released forced layers to detach and migrate in solution [157]. Indeed, Li-ion-based intercalation is the most popular intercalation method used to produce SAs based on MoS_2 [90], WS_2 [94, 95], Bi_2Te_3 [17, 38, 106, 148–155], and Bi_2Se_3 [112, 113]. Sodium ions can also be used in a process involving hydrazine initially, which releases ammonia (NH_3), H_2, and nitrogen (N_2) gases while intercalating the TMD layers, then an Na-naphthalenide solution is added in a second step [93, 158]. Intercalation by electrochemistry is an exfoliation process in which the layered material acts as an electrode in an electrochemical setup [56], which has also been used to produce SAs. For example, graphite can be used as anode with platinum (Pt) as cathode in an electrolyte solution to produce graphene monolayers [159–161, 68]. In such experiments, sulfuric acid or sulfate salts were used and sulfate was the intercalated ion. A similar process was used to produce BP-based SAs, with the crystal used as cathode (with a Pt foil anode) with tetra-*n*-butyl-ammonium bisulfate as electrolyte in anhydrous deoxygenated propylene carbonate [131, 132].

A chemical modification of the layers has proved to be a very popular method to exfoliate graphene in water, avoiding the use of surfactants. The material obtained has oxygen-containing functional groups [58], making it easily soluble in water, and is so called graphene oxide (GO), which is different from the graphene obtained in the liquid phase by other methods discussed above. This is usually carried out using the Hummers method, consisting of treatment in sulfuric acid and potassium permanganate [57]. Other oxidization routes include nitric acid or other oxidizing agents like potassium chlorate [58]. GO can be used as such to make SAs [18, 40, 69–76, 82, 162]. GO can be reduced back to graphene by hydrazine [163]. As reduction is never complete, this material is known as reduced GO (RGO), to distinguish from pristine graphene, which can also be used to make SAs [77–82].

2.2 Stabilization methods

Once exfoliated, 2DMs need to be stabilized in the liquid phase to avoid reaggregation. Stabilization methods are 2DM dependent and can involve the use of a suitable solvent, surfactants, or polymers, to minimize the exfoliation energy cost [55]. Organic solvents like *N*-methyl-2-pyrrolidone (NMP) and dimethyl formamide (DMF) have successfully been employed for the liquid-based exfoliation of a number of 2DMs, like graphene [133], TMDs [135, 164], and BP [165–167]. It has been proposed that exfoliation in a solvent is successful as long as some solubility parameters, like surface tension and Hildebrandt or Hansen parameters, are very close for the solvent and the material [55, 133, 135, 146]. This enhances the compatibility between the material and the solvent, and increases the material concentration in solution [55, 133, 135, 146]. Other solvents used for graphene were ortho-dichlorobenzene [168] and perfluorinated aromatic solvents [169]. Among the solvents used for fabricating SAs, NMP is the most popular [61, 67, 88, 103, 116, 117, 119–129, 144, 145], while other solvents used are DMF [85–88] and isopropyl alcohol (IPA) [42, 89, 104, 116–118]. While the main advantage of using solvents is the high purity of the final material, there are also several drawbacks. Indeed, NMP and DMF are toxic and their high boiling point prevents an easy removal [55]. Also, solvents may not be compatible with further steps of a process [55]. While other solvents with lower boiling points have been proposed, like acetone, acetonitrile, 1-propanol, or IPA, their solubility parameters were not as good as those for NMP and DMF and their use was not as successful [170–174]. Despite this, there are a number of reports on SAs made from IPA-based 2DM solutions, particularly MoS_2 [89], PtTe [104], Bi_2Se_3 [16, 89, 110, 111, 137, 138], and BP [42, 116–118].

The use of surfactants (i.e. cationic, anionic, or non-ionic molecules with a long non-polar tail and a polar or

charged head) in water provides a viable alternative to exfoliation in organic solvents [55, 56]. In this approach, the long non-polar tail of the surfactant adsorbs on the layered material, also non-polar. The polar or ionic head is instead exposed to water, also polar, thus stabilizing the solution and also preventing aggregation by electrostatic or steric repulsion [55]. This method has been mainly adopted for graphene, using sodium dodecylbenzene sulfonate, sodium cholate, sodium deoxycholate, cetyltrimethylammonium bromide, and tetracyanoquinodimethane [61, 134, 175–177]. TMDs have also been dispersed in water using SC [178].

Due to the convenience of operating in aqueous environment, surfactants have been widely used in processes for fabricating SAs [19, 36, 39, 41, 60, 61, 63–66, 83, 84, 91, 92, 96, 99, 130]. While the use of water as a solvent makes the processing environmentally friendly and harmless, as well as potentially compatible with subsequent steps, the final material is not pure and may require a further processing step in case the surfactant causes interference with the designated application. When 2DMs are to be used as SAs, absorption of the surfactants in the laser region should be taken into account. Surfactants are usually transparent in the visible range but may give some optical absorption in the near-infrared region, where they may then cause non-saturable losses in the laser cavity. Hence, for fiber laser applications, they must be chosen carefully depending on the output wavelength or removed from the final SA material. Beyond the specific SA applications, surfactants must also be removed if, for example, graphene dispersions are to be used for making transparent conductive films. In this case, surfactant molecules prevent efficient contact between flakes, thus increasing junction resistance, impeding efficient carrier hopping from flake to flake and ultimately increasing the overall film resistance [179]. However, an easy solution is just washing the surfactant away with water to minimize junction and the overall sheet resistance [179]. Hence, surfactants are potentially detrimental not just for optical applications but also for electrical ones.

The use of polymers is also a valid approach to the stabilization of 2DMs in both water and organic solvents. In general, polymers are partially adsorbed onto the material's surface, leaving segments protruding into the liquid and preventing reaggregation by steric repulsion [55, 180]. However, this approach has found only limited applications for SA fabrication, as only in one case has polyvinyl alcohol (PVA) been reported as both a stabilizing polymer and polymer matrix for fiber laser integration [62].

2.3 Sorting methods

Regardless of the exfoliation and stabilization method, a final sorting step is always needed to enrich the solution of single- or few-layer material with the desired flake size. The universal sorting technique is centrifugation. Standard centrifugation can also be referred to as sediment-based separation. During this process, the fragmented 2DMs separate according to their size and thickness. Thick and large flakes sediment faster and are thus found in the bottom at the end of the process [55].

Standard centrifugation is the only sorting method used within SA fabrication. However, variations of the standard centrifugation exist. Density gradient ultracentrifugation allows a more precise control on the number of layers and lateral size [181–183], where flakes separate according to their density through a density gradient. However, this process is time consuming and has a very low yield, and thus is not useful for practical applications, including SAs.

A centrifugation method with good size and thickness control as well as higher yield than density gradient ultracentrifugation is liquid cascade centrifugation [184], which has been developed for TMDs but can be used in principle for any 2DMs. In this method, a solution containing the exfoliated and stabilized material is subjected to subsequent centrifugation steps, where the sediment is separated and redispersed and the supernatant is centrifuged again at a higher speed. This is repeated multiple times with speeds that can be tuned according to the desired size and thickness distribution [184]. This is a recently developed method that has not found application in SA fabrication yet; however, we cannot rule out its application in the near future.

2.4 MXene fabrication

MXenes are not typically produced by the common LPE methods. These are carbides or nitrides (or carbonitrides) of early transition metals, of which the most popular is titanium [185]. MXenes are obtained from the so-called MAX phases, also containing a layer of a group IIIA element, normally Al. Such MAX phases can be treated with hydrofluoric acid (HF) to etch the Al layer and leave the exfoliated MXene sheets in solution [185]. MXenes can be prepared by top-down or bottom-up methods such as aqueous acid etching (AAE), high-temperature etching, and CVD method, of which AAE is the most commonly used method in the preparation of high-quality MXenes

[186]. AAE is the etching of element A in the MAX phase by using acid solution, while MXenes are usually exfoliated by an ultrasonic method [187]. In this process, HF solution is the most attractive etchant for researchers due to its advantages of mature process, high practicability, and low cost [188]. For example, Wu et al. and Jhon et al. obtained $Ti_3C_2T_x$ and Ti_3CNT_x by etching Al layers from different MAX phases in 40% and 30% HF acid, respectively [189, 190]. Because intercalation cations such as NH_4^+ and K^+ can facilitate etching and exfoliation, fluorohydrides (e.g. NH_4HF_2 and KHF_2) are also popular etchants for fabricating MXenes [191].

2.5 Fabrication summary

Table 1 shows a summary of fabrication methods for SAs. Notably, ultrasonication maintains its popularity as an exfoliation method; however, intercalation is still significantly used to fabricate SAs. The intercalation process relies on chemistry (or electrochemistry) to produce exfoliated layers, and as such may cause their chemical modification and ultimately an alteration of the electronic and optical properties, which is an effect that should be taken into account when fabricating an SA. Conversely, ultrasonication only relies on physical forces and maintains the layer structure intact [53, 55, 56]. We thus believe that this is a preferable exfoliation method. When ultrasonication is used, we notice that the applications of surfactant and solvents are roughly evenly split. This is because both have their own distinct advantages and disadvantages, as mentioned above. When intercalation is used, the most popular option is based on lithium ions.

3 Solution-processed 2DM-based ultrafast fiber lasers

Fiber lasers are attractive platforms for ultrafast pulse generation due to their advantages of high pulse quality, flexibility, and compactness [1, 2]. Meanwhile, the use of SAs is a preferred method for the generation of pulses in fiber lasers [30]. Particularly, 2DM-based SAs are more attractive in terms of their broadband operation and engineerable properties [23]. Indeed, solution-processed 2DMs have been widely exploited in fiber lasers, as evident from Table 2. Here, we summarize the common 2DMs used and the current trends.

3.1 Graphene

Since the first demonstration of graphene-mode-locked fiber lasers based on solution processing [37], solution-processing-based graphene has been widely used for mode locking fiber lasers in the 1-μm [62], 1.5-μm [36, 41], and 2-μm regions [66]. For example, Hasan et al. obtained 630-fs pulse at 1.56 μm by LPE of graphite [61]. Besides, polymer composites are a common carrier that is used to integrate graphene into fiber lasers [18]. In 2010, Sun et al. reported a wavelength-tunable (1525–1559 nm) fiber laser based on graphene PVA composite [41]. Popa et al. obtained 173-fs pulse from a dispersion-managed Er-doped fiber laser mode-locked by graphene PVA composite [63]. Apart from PVA [36, 41, 62–66, 69], some other polymers have also been exploited to fabricate graphene-based films. In 2009, Zhang et al. demonstrated mode-locked Er-doped fiber lasers based on graphene polyvinylidene fluoride polymer membrane [18]. In 2011, Gui et al. reported a self-assembled graphene membrane as an ultrafast mode locker in an Er-doped fiber laser [77]. In 2016, Torrisi et al. proposed graphene-styrene methylmethacrylate composite for ultrafast lasers [67]. The method of optical deposition is also used to transfer graphene to the fiber in laser cavity [78–81, 162]. For instance, Fu et al. reported a graphene-mode-locked Er-doped fiber laser based on optical deposition, where a fiber connector for physical contact (FC/PC) was immersed in graphene solution. After alcohol evaporation, a graphene film was obtained at the center of the fiber core on the FC/PC tip, as shown in the inset of Figure 2A. They obtained the bound states of solitons and harmonic mode locking (HML) with orders from 1st to 26th [81]. Figure 2B shows a spectrum of HML (inset, pulse profile). Similar to optical deposition, Lin et al. embedded graphene nanoparticles into photonic crystal fiber (PCF), which achieves the evanescent wave mode locking in an Er-doped fiber laser [68].

As a graphene derivative, GO has been widely investigated as a broadband SA candidate because of its ultrafast recovery time, flat saturable absorption, low cost, and easy preparation [40, 200]. In 2010, GO-based fiber laser was first reported by Bonaccorso et al., who achieved an ~743-fs pulse in an Er-doped fiber laser [201]. PVA as a polymer matrix was also popular in GO-based ultrafast fiber lasers [70–72]. Besides, Liu et al. demonstrated a nanosecond pulse by using few-layered GO SA, where a hollow core PCF was filled with GO solution [73]. Xu et al. obtained 200-fs pulses in a dispersion-managed fiber laser, where a thin GO membrane was formed on the broadband reflective mirror [40]. Jung et al. achieved a mode-locked fiber laser at 2-μm band by spraying GO onto the flat side of

Table 2: Summary of the typical ultrafast fiber lasers enabled by solution-processed 2DMs.

Material type	Fabrication method[a]	Incorporation method[b]	Laser type[c]	α_s (%)	I_{sat} (MW/cm^2)	λ (nm)	τ (s)	f_{rep} (Hz)	SNR (dB)	Energy (mW/J)	Ref.
Graphene	LPE	PVA	EDFL	4.5	266	1525–1559	1 p	8 M	80	1/125 p	[41]
Graphene	RGO	PVDF	EDFL	28.3	0.75	1589.68	694 f	6.95 M	65	20.85/3 n	[18]
Graphene	LPE	PVA	EDFL	5	266	1562	970 f	19.9 M	–	–/–	[61]
Graphene	LPE	SMMA	EDFL	0.9	140 μJ/cm^2	1550	502 f	–	–	–/–	[67]
Graphene	RGO	OD	EDFL	7.6	2.675 GW/cm^2	1562.26	950 f	502.84 M	50	2.3/4.6 p	[80]
Graphene	RGO	OD	EDFL	6.6	–	1558	950 f	15.75 M	70	0.18/11.2 p	[81]
GO	GO	SAM	EDFL	2.6	60	1556.9	600 f	25.6 M	50	3.3, 5.8	[40]
						1560	200 f	22.9 M	60	0.13 n, 0.25 n	
GO	GO	Filling PCF	EDFL	8	3.5 mW	1561.2	4.85 n	7.68 M	81	4.3/0.56 n	[73]
GO	GO	DSF	TDFL	–	–	1910	1.3 p	15.9 M	47	–	[75]
GO	GO	DSF	THDFL	7.1	14.83 W	1950	578 f	33.25 M	50	–/4.3 n	[74]
GO	GO	SAM	EDFL	2.6	60	1531	11 p	19.5 M	65	23.3/1.2 n	[192]
Bi_2Se_3	LPE	OD	YDFL	3.8	53	1067.66	1.95–8.3 μ	8.3–29.1 k	48	0.46/17.9 n	[136]
Bi_2Se_3	LPE	NMP	EDFL	3.8	53	1530.3	4.9–24 μ	6.2–40.1 k	50	1.6/39.8 n	[59]
Bi_2Se_3	PM	PVA	EDFL	~3.9	12	1557.5	660 f	12.5 M	55	1.8/0.144 n	[89]
Bi_2Se_3	LPE	PVA	Pr-doped ZBLAN	3.7	41	604	497–748 n	86.2–187.4 k	40	7.7/3.1 n	[109]
Bi_2Se_3	PM	OD	EDFL	41.20	101.8	1565.14	13.4–36 μ	4.508–12.88 k	55	112 μW/13.3 n	[16]
Bi_2Se_3	LPE	OD	TM-DCFL	3.7	41	1980	4.18 μ	8.4–26.8 k	43	8.4/313 n	[193]
Bi_2Se_3	PM	IPA	YDFL	5.2	70 μJ/cm^2	1031.7	46 p	44.6 M	58	33.7/0.756 n	[111]
Bi_2Se_3	PM	PVA	YDFL	11.05	17.4	1036	7.2–11.6 μ	86.2–137.8 k	35 dBm	4.6, 1.88	[138]
		OD		9.2	14.9	1554.56	507 p	17.7 M	44 dBm	34.2 n, 0.1 n	
Bi_2Se_3	HIE	CaF_2 substrate	Ho-doped ZBLAN	51.3	2.12	2979.9	1.37–4.83 μ	46.20–81.96 k	37.4	327.38/3.99 μ	[17]
Bi_2Te_3	HIE	PVA	EDFL	2	180	1557	1.08 p	8.635 M	60	0.25/29.0 p	[151]
Bi_2Te_3	LPE	OD	EDFL	22	57	1510.9–1589.1	13–49 μ	2.154–12.82 k	36.4	238.5/1.525 μ	[153]
Bi_2Te_3	HIE	Filling PCF	YDFL	19.1	14.9	1064.47	960 p	1.11 M	60	–/–	[106]
Sb_2Te_3	LPE	DSF	EDFL	3.9	106	1556	449 f	22.13 M	74	0.9/39.6 p	[115]
MoS_2	HIE	EF	EDFL	2.82	–	1556.86	–	6.77 M	–	65 μW/9.6 p	[98]
MoS_2	HIE	PVA	EDFL	4.3	34	1569.5	710 f	12.09 M	60	1.78/0.147 n	[194]
MoS_2	LPE	PVA	EDFL	10.69	2.02	1535–1565	0.96–7.1 p	12.99 M	55	0.844/65 p	[19]
MoS_2	HIE	EF	YDFL	10.47	0.88 mW	1042.6	656 p	6.74 M	59	2.37/0.352 n	[93]
MoS_2	LPE	DMF	Pr-doped	–	–	604	602–1955 n	50.8–118.4 k	39	0.6, 0.7	[88]
/WS_2		NMP	ZBLAN				435–1101 n	67.3–132.2 k	41	5.5 n, 6.4 n	
MoS_2	LPE	PVA	YDFL	1.6	13	1066.5	5.8 μ	6.4–28.9 k	44.6	0.9, 1.7, 47.3	[87]
			EDFL			1565	23.3–5.4 μ	6.5–27.0 k	54.5	/32.6 n, 63.2 n	
			TDFL			2032	1.76 μ	33.6–48.1 k	54.6	1 μ	
$MoSe_2$	LPE	PVA	THDFL	4.4	25.7 W	1912.6	920 f	18.21 M	65	4.3/0.24 n	[141]
$MoSe_2$	Bath type sonication	DSF	EDFL	5.4	24	1557.3	737–798 f	15.38 M–3.27 G	61.9	0.23–22.8	[142]

Table 2 (continued)

Material type	Fabrication method[a]	Incorporation method[b]	Laser type[c]	α_s (%)	I_{sat} (MW/cm^2)	λ (nm)	τ (s)	f_{rep} (Hz)	SNR (dB)	Energy (mW/J)	Ref.
				4.2	43 W					5.9–14.6 p	
WS_2	LPE	DSF	THDFL	10.9	1.9 W	1941	1.3 p	34.8 м	72	0.6/17.2 p	[195]
WS_2	LPE	PVA	YDFL	3.1	1.38	1030	3.2–6.4 μ	24.9–36.7 k	53	0.5, 16.4	[39]
			EDFL	4.9	3.83	1558	1.1–3.4 μ	79–97 k	44	13.6 n, 179.6 n	
WS_2	Thermal decomposition	Fluorine mica film	YDFL	5.8	–	1053	713 p	23.26 м	55	–/–	[196]
WSe_2	LPE	PVA	EDFL	3.5	103.9	1560	3.1–7.9 μ	4.5–49.6 k	46.7	1.23/33.2 n	[99]
TiS_2	LPE	EF	EDFL	8.3	1.2 mW	1563.3	812 f	22.7 м	60	0.574/25.3 p	[100]
SnS_2	LPE	PVA	YDFL	0.76	78	1062.66	656 p	39.33 м	53	2.23/0.057 n	[101]
SnS_2	LPE	PVA	EDFL	4.6	125	1562.01	623 f	29.33 м	45	1.2/0.041 n	[102]
ReS_2	LPE	PVA	EDFL	0.12	74	1557.3	5.496–23 μ	12.6–19 k	46	1.2/62.8 μ	[103]
$PtTe_2$	LPE	PVA	YDFL	–	–	1066	5.2–13.6 μ	23.0–33.5 k	35	2.48/74 n	[104]
BP	LPE	CHP	EDFL	3.45	~50	1555	1.06 p	37.8 м	80	–/–	[197]
BP	LPE	Au mirror	HDFL	41.2	3.767	2970.3	2.41 μ	62.5 k	37.7	308.7, 87.8	[116]
			HPDFL			2866.7	8.6 p	13.987 м	56	4.93 μ, 6.28 n	
BP	LPE	PVA	EDFL	8.3	7.9	1565.3–1567.8	1.365–3.39 μ	64.51–82.64 k	>75	12.03/148.63 n	[127]
BP	LPE	SAM	Er-doped ZBLAN	15	9 μJ/cm^2	2779	1.18–2.1 μ	39–63 k	35	485/7.7 μ	[117]
BP	LPE	EF	EDFL	10.1	9.27	1549–1575	280 f	60.5 м	68	–/–	[118]
BP	LPE	Inkjet-printed	EDFL	~10.03	~14.98	1555	102 f	23.9 м	>60	1.7/71 p	[129]
BP	LPE	PVA	EDFL	~0.35	–	~1558	~700 f	~20.82 м	>60	~1.5/ ~0.07 n	[128]
BPQDs	LPE	EF	EDFL	8.1	1.69 mW	1561.7	882 f	5.47 м	~67	135 μW/24.7 p	[119]
BPQDs	LPE	EF	EDFL	9.0	1.5	1562.8	291 f	10.36 м	>50	–/–	[120]
BPQDs	Solvothermal	PVDF	EDFL	36	3.3 GW/cm^2	1567.5	1.08 p	15.22 м	64.3	–/–	[198]
Ti_3CNT_x	AAE	DSF	EDFL	1.7	45 W	1557	660 f	15.4 м	60	0.05/3.25 p	[190]
$Ti_3C_2T_x$	AAE	DSF	YDFL	38.3	69.3 GW/cm^2	1065.89	480 p	18.96	56	9, 3	[186]
			EDFL	2.0, –	37.5 GW/cm^2	1555.01	159 f	7.28 м	62	0.47 n, 0.41 n	
$Ti_3C_2T_x$	AAE	EF	EDFL 1	11.3	1.94 mW	1564.24	597.8	17.9	55.2	0.283, 1.3	[189]
			EDFL 2			1550	104 f	20.03 м	62.4	15.8 n, 64.9 p	
$Ti_3C_2T_x$	AAE	OD	EDFL	2.8	191	1565	1.37–3.19 μ	99.6–131.1 k	61	40/305 n	[188]
Ti_2CT_x	AAE	Film deposition	YDFL			1051.08	164.4 p	11.2 м	57.1	80/0.81 μ	[199]
			EDFL	23.1	4.2	1565.4	5.3 p	8.25 м	62		
			Er-doped ZBLAN	15.7	5.1	2798	730 n –1.83 μ	44.1 k –99.5	33.1		

α_s, modulation depth; I_{sat}, saturation intensity; λ, wavelength; τ, pulse width; f_{rep}, repetition frequency; SNR, signal-to-noise ratio.

[a]Fabrication method: liquid-phase exfoliation (LPE), polyol method (PM), hydrothermal intercalation/exfoliation (HIE), aqueous acid etching (AAE).

[b]Incorporation method: saturable absorber mirror (SAM), polyvinyl alcohol (PVA), polyvinylidene fluoride (PVDF), styrene methylmethacrylate (SMMA), optical deposition (OD), photonic crystal fiber (PCF), D-shaped fiber (DSF), *N*-methyl-2-pyrrolidone (NMP), isopropyl alcohol (IPA), evanescent field (EF), dimethyl formamide (DMF), cyclohexyl pyrrolidone (CHP).

[c]Laser type: Yb-doped fiber laser (YDFL), Er-doped fiber laser (EDFL), Tm-doped fiber laser (TDFL), Tm, Ho-codoped fiber laser (THDFL), Ho-doped fiber laser (HDFL), Ho, Pr-codoped fiber laser (HPDFL), Tm-doped double-clad fiber laser (TM-DCFL).

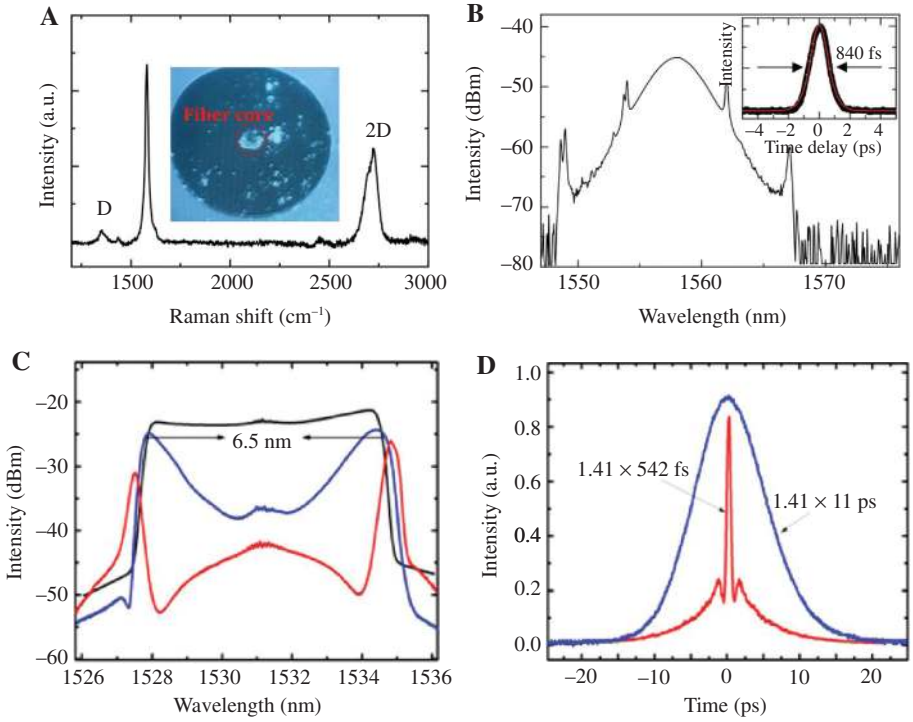

Figure 2: Mode-locked results enabled by graphene and GO.
(A) Raman spectrum of the graphene (inset: graphene optically deposited on fiber tip). (B) HML spectrum (inset: the autocorrelation trace of the 26th harmonic). (C) Spectra: before pulse compression (black curve), after 50-m single-mode fiber (blue curve), and after 75-m single-mode fiber (red curve). (D) Autocorrelation trace of chirped (blue curve) and dechirped pulses (red curve). (A) and (B) are reproduced with permission from Ref. [81]. Copyright 2019 CLP Publishing. (C) and (D) are reproduced with permission from Ref. [192]. Copyright 2012 OSA Publishing.

a D-shaped fiber [74, 75]. Xu et al. reported dissipative soliton generated from a GO-mode-locked fiber laser, in which a broadband reflective mirror was immersed into the GO hydrosol for 48 h [192]. Figure 2C shows the spectra before pulse compression (black curve), after 50-m single-mode fiber (blue curve) and after 75-m single-mode fiber (red curve). Figure 2D shows the autocorrelation trace of chirped (blue curve) and dechirped pulses (red curve). Lee et al. reported a Q-switched mode-locked fiber laser by depositing GO to a D-shaped fiber [76]. Sobon et al. compared the properties of GO with RGO as SAs in Er-doped mode-locked fiber laser, and showed that GO could be an efficient SA without reduction to RGO [82].

Although the modulation depth of single-layer graphene is ~2.3% or less [33, 36, 67], it can be easily enhanced by increasing the number of layers [33]. Furthermore, broadband operation is another remarkable property of graphene [41]. For example, Fu et al. achieved a broadband mode-locked fiber laser by using a single graphene SA at different wavelengths, where the span of the wavelength covers from Yb-doped (1 μm), Er-doped (1.5 μm), and Tm-doped (2 μm) (up to 1000 nm) [31]. Graphene started a new beginning for 2DM-based ultrafast photonics, paving the way for the research and development of ultrafast lasers enabled by 2DMs [20].

3.2 Topological insulators

Similar to graphene, TIs such as Bi_2Se_3, Bi_2Te_3, and Sb_2Te_3 belong to the Dirac materials [202]. In 2012, TI-based SA was first reported in an Er-doped fiber laser [38]. Panels A and B of Figure 3 show the scanning electron microscopy (SEM) and transmission electron microscopy (TEM) images of the Bi_2Te_3 nanosheets fabricated by the method of hydrothermal intercalation/exfoliation. The mode-locked spectrum and corresponding autocorrelation trace are shown in Figure 3C and D, respectively. Since then, hydrothermal intercalation/exfoliation has been widely used to produce TIs [17, 38, 112, 148–150]. For example, Wu et al. reported on 635-nm visible Q-switched Pr-doped ZBLAN fiber lasers with Bi_2Se_3 and Bi_2Te_3 SAs [105]. Li et al. experimentally demonstrated a 212-kHz-linewidth transform-limited pulse from a single-frequency Q-switched fiber laser based on a few-layer Bi_2Se_3 SA [107]. For TI integration into the laser cavities, polymer matrices

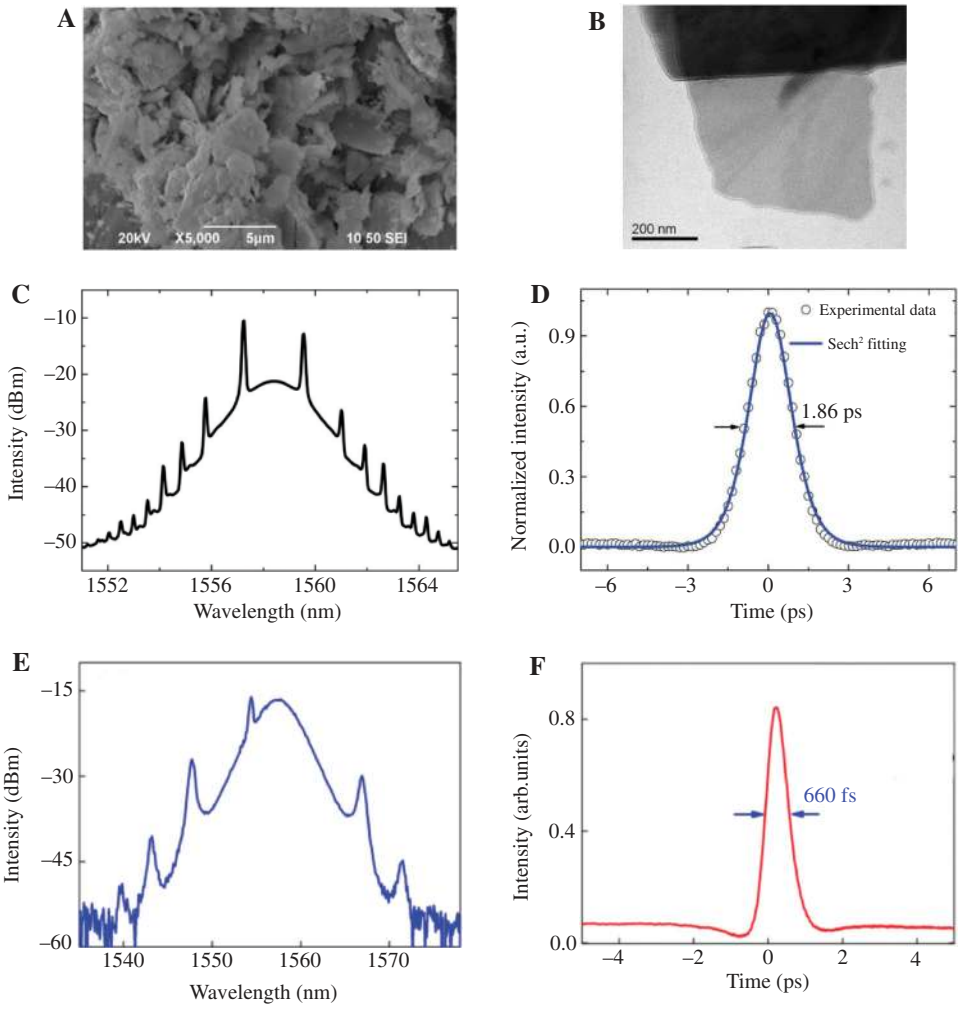

Figure 3: Mode-locked results enabled by Bi_2Te_3 and Bi_2Se_3.
(A) SEM and (B) TEM images of the Bi_2Te_3 nanosheets prepared by hydrothermal intercalation/exfoliation. (C) Spectrum and (D) autocorrelation trace. (E) Spectrum and (F) autocorrelation trace of mode-locked fiber laser based on Bi_2Se_3. (A)–(D) are reproduced with permission from Ref. [38]. Copyright 2012 AIP Publishing. (E) and (F) are reproduced with permission from Ref. [89]. Copyright 2014 OSA Publishing.

such as PVA were frequently utilized in the preparation of TI-based SAs [89, 108, 109, 137, 151]. In 2014, Liu et al. obtained 660-fs pulses generated in an Er-doped fiber laser enabled by Bi_2Se_3 nanosheets [89]. The spectrum and autocorrelation trace are shown in Figure 3E and F, respectively. In 2015, Mao et al. integrated Bi_2Te_3-PVA films into an Er-doped fiber laser and obtained mode-locked pulses at a low pump power of ~13 mW [151]. Optical deposition is also suitable for transferring TIs to the fiber tips in laser cavity [16, 113, 152–155, 193, 203]. In 2013, Chen et al. proposed a self-assembled Bi_2Se_3-based membrane as an SA, which achieved dual-wavelength Q-switched pulses in Er-doped fiber laser [16]. In 2014, Liu et al. obtained dual-wavelength harmonic-mode-locked pulses with Bi_2Te_3-based microfiber [154]. In 2018, Jin et al. reported on 3.125-GHz harmonics realized by Bi_2Te_3-based tapered fiber by optical deposition [155]. In addition, polyol method was also used to prepare TIs as SAs in fiber lasers [110, 111, 138]. For example, Zhao et al. reported a wavelength-tunable picosecond soliton pulse generated in a Bi_2Se_3 mode-locked fiber laser [110]. Dou et al. exploited Bi_2Se_3 as SA to achieve mode locking in a Yb-doped fiber laser [111]. Lin et al. obtained Q-switched pulses in a Yb-doped fiber laser by Bi_2Se_3 [138]. Besides, some other methods such as TI-based solution filled in PCF were also used to achieve mode locking in fiber lasers [106, 114].

TIs have a broad non-linear response and a large modulation depth [23]; however, the mode-locking stability is, to some extent, lower than graphene. Sometimes, the signal-to-noise ratio of the mode-locked fiber lasers based on TIs SAs are <60 dB [89, 108, 111, 137]. In addition, TI-based SAs tend to obtain Q-switched pulses with pulse width

in the order of nanoseconds or microseconds [16, 109], which is undesirable as it is usually preferred to achieve ultrashort pulses (picoseconds or sub-picoseconds) for applications in optical communications and material processing [89, 114]. Therefore, it is of vital importance to make TI-based SAs with better performance in order to further optimize the mode-locking properties.

3.3 Transition metal dichalcogenides

TMDs, such as MoS_2, $MoSe_2$, WS_2, and WSe_2, have a layer-dependent bandgap that allows them to be used as broadband SAs in ultrafast fiber lasers [90]. Since Zhang et al. first demonstrated MoS_2 as an SA in passively mode-locked fiber laser by optical deposition [90], ultrafast fiber lasers enabled by TMD-based SAs have been extensively investigated. Several techniques were used for the preparation of TMDs as SAs in fiber lasers [194, 195, 204]. In 2013, Wang et al. revealed the ultrafast saturable absorption of 2D MoS_2 nanosheets by using the LPE technique, indicating that MoS_2 is a potential SA for achieving ultrafast fiber lasers [34]. In 2014, Luo et al. reported Q-switched fiber lasers operated at 1, 1.5, and 2 μm by sandwiching the MoS_2 PVA film between two fiber ferrules, which shows the broadband properties of MoS_2 as an SA for ultrafast photonics [87]. In 2015, Woodward et al. obtained stable Q-switched pulses at 1060, 1566, and 1924 nm in Yb-, Er-, and Tm-doped fiber lasers, respectively, by embedding liquid-phase exfoliated few-layer $MoSe_2$ flakes into a polymer film [60]. Mao et al. reported on WS_2-mode-locked fiber lasers, where WS_2 nanosheets were deposited on a D-shaped fiber and WS_2 PVA film was sandwiched into the facet of the fiber connector [97]. Li et al. proposed a WS_2-based SA fabricated by the thermal decomposition method, which achieves sub-nanosecond mode-locked pulses in Yb-doped fiber laser [196]. Chen et al. obtained Q-switched pulses based on four kinds of TMD PVA materials (MoS_2, $MoSe_2$, WS_2, and WSe_2) with the same cavity configurations [84]. Panels A–D of Figure 4 show the spectra of MoS_2, $MoSe_2$, WS_2, and WSe_2, respectively. In fact, while several TMDs have been obtained by solution processing [135], researchers are devoting significant effort to explore such new TMDs for applications in ultrafast photonics [35, 91, 100–104, 205]. In 2017, Mao et al. reported on a passively Q-switched and mode-locked fiber laser based on a film-type ReS_2 PVA, demonstrating that ReS_2 has similar saturable absorption property to MoS_2

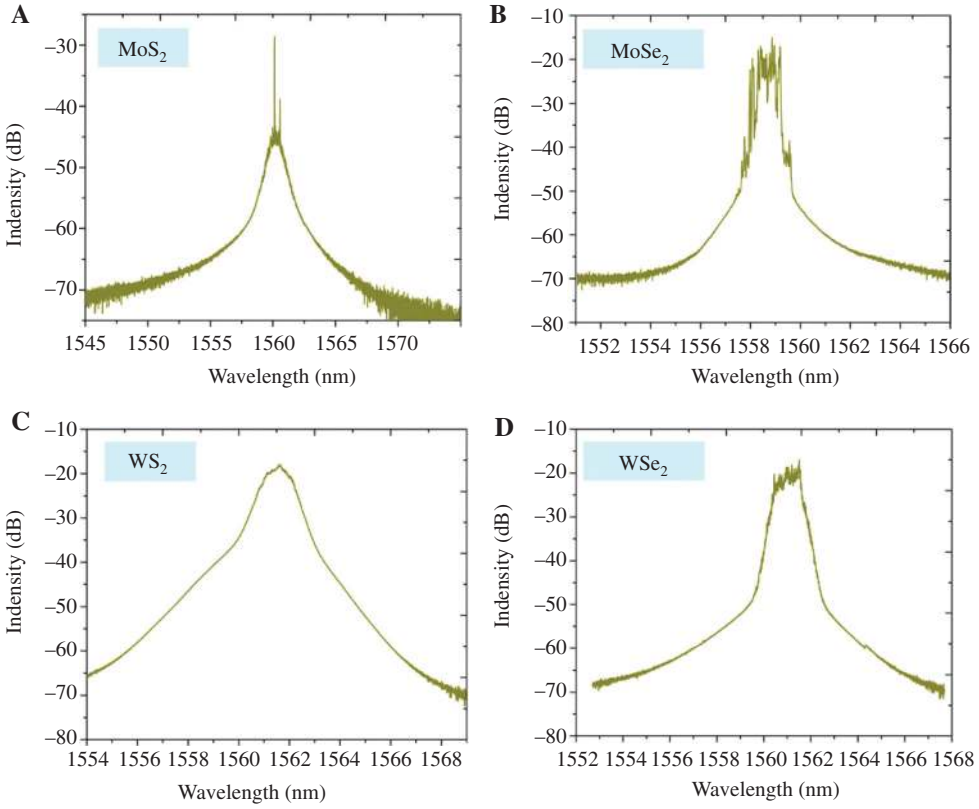

Figure 4: Q-switched spectra enabled by TMD-based SAs.
(A) MoS_2, (B) $MoSe_2$, (C) WS_2, and (D) WSe_2. Reproduced with permission from Ref. [84]. Copyright 2015 OSA Publishing.

and WS_2 [103]. In 2018, Tian et al. reported a femtosecond mode-locked fiber laser with TiS_2 based on LPE, indicating that non-equilibrium electrons could promote TiS_2-based SA to be an ultrafast switch for ultrafast pulse output [35]. In 2018, Niu et al. reported a passively mode-locked Er-doped fiber laser based on SnS_2 PVA film, where a long-time and stable mode locking was achieved [102]. Wang et al. reported that a high-energy passively Q-switched Er-doped fiber laser enabled $Mo_{0.5}W_{0.5}S_2$-based SA, where the $Mo_{0.5}W_{0.5}S_2$-alcohol solution was injected into the quartz tube in order to deposit it onto the taper fiber [91]. In 2019, Cheng et al. suggested a multilayer $PtTe_2$ PVA composite thin film as an SA, achieving Q-switched pulses in a Yb-doped fiber laser [104].

A variety of TMD materials have been discovered, where MoS_2 and WS_2 are the most common SAs that were used to achieve ultrashort pulses. PVA composites usually serve as carriers for transferring TMDs to the laser cavity. Meanwhile, the method of evanescent field is an alternative way to accomplish the interaction between lasers and TMDs. Similar to TIs, TMD-based SAs also easily produce Q-switched pulses. Thus, it is important to fabricate better TMD materials to improve the performance of lasers.

3.4 Black phosphorus

In 2014, BP joined the family of 2DMs [206]. The bandgap of BP ranges from 0.3 eV (bulk) to 2.0 eV (monolayer) and the energy bandgap depends on its thickness [207]. The broadband non-linear optical response of BP was confirmed by the wideband open-aperture Z-scan measurement technique from the visible to mid-infrared region [208]. Since the first demonstration of BP-based passively mode-locked fiber lasers [209], BP has been used to mode lock fiber lasers in the 1-μm [42, 131], 1.5-μm [119–121, 125, 197], and 2-μm regions [122, 144] by the solution-processing method, as well as to Q-switch fiber lasers [116, 123, 126, 127, 130, 132, 210]. For example, Qin et al. reported on BP fabricated by LPE for the Q-switched Er:ZBLAN fiber laser at 2.8 μm, where the maximum average power of 485 mW with pulse energy of 7.7 μJ was achieved [117]. Luo et al. proposed a lateral interaction mechanism based on BP-based microfibers by the LPE in an Er-doped fiber laser [124]. They believed that this mechanism not only increases the damage threshold of several layers of BP as SA but also increases the interaction between light and matter [124]. Chen et al. reported on sub-300-fs tunable fiber laser with all-anomalous dispersion mode locked by BP, in which the multi-layer BP was deposited on the tapered fiber by the method of evanescent field interaction [118]. Jin et al. obtained a long-term stable ultrashort pulse (~100 fs) generated in a BP mode-locked fiber laser by a scalable and highly controllable inkjet printing technology [129]. Song et al. achieved a vector soliton fiber laser by incorporating BP nanoflake-based SA into an Er-doped fiber laser, indicating that nanoflake-based BP SAs were polarization independent and suitable for vector soliton fiber laser [145]. Panels E and F of Figure 5 show the spectra and autocorrelation trace of vector soliton fiber laser mode locked by BP. Furthermore, Yun reported a dual-wavelength polarization-locked vector soliton in an Er-doped fiber laser enabled by BP-based PVA film [128]. Xu et al. exploited black phosphorene quantum dots (BPQDs) as a mode-locker in an Er-doped fiber laser, indicating that BPQDs have potential applications for ultrafast photonics [198]. Figure 5A shows the TEM of BPQDs prepared by a solvothermal method in NMP solution, and the absorption trace is shown in Figure 5B. Panels C and D of Figure 5 show the spectrum and autocorrelation trace, respectively. It is worth noting that BPQDs as SAs demonstrated better performance than BP nanosheets due to quantum confinement effects [198].

PVA composites and evanescent filed interaction are the typical methods to incorporate BP to the laser cavity. BP has a low saturation intensity and the ability of broadband operation up to the ~3-μm band [120, 208]. BP-based SAs such as BPQDs and black phosphorene nanoparticles have also been exploited to achieve ultrashort pulses in fiber lasers [119–121]. However, BP is not stable enough and easily oxidized in the air. Different preparation methods have been studied to obtain the BP-based SAs with the best performance. For example, Hu et al. proposed a printed BP ink in order to improve the long-term stability (~30 days) of the BP devices [211]. For now, the fabrication of BP with higher stability and quality is still a big challenge.

3.5 MXenes

Recently, MXenes (2D transition metal carbides, carbonitrides, or nitrides [20]) have attracted more attention because of their outstanding optoelectronic and optical properties [185, 212, 213]. In 2017, John et al. reported Ti_3CNT_x-based SA by solution processing in an Er-doped fiber laser, where the stacked Ti_3CNT_x monolayers were transferred to a side-polished fiber, and obtained stable pulses as short as 660 fs at a repetition rate of 15.4 MHz and a wavelength of 1557 nm [190]. In 2018, Jiang et al. investigated the broadband non-linear photonics of $Ti_3C_2T_x$ by depositing $Ti_3C_2T_x$ solution onto a side-polished fiber [186], where stable mode locking was achieved in Yb- and Er-doped fiber lasers, respectively, as shown in Figure 6.

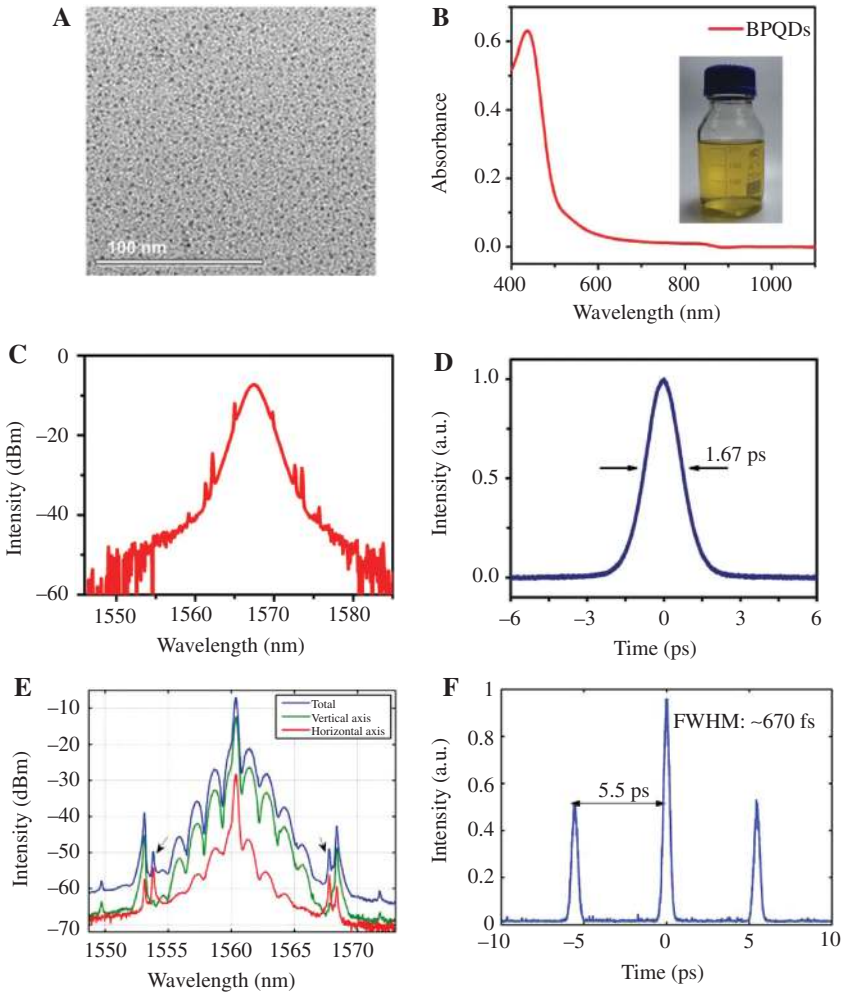

Figure 5: Mode-locked results enabled by BP-based SAs.
(A) TEM image and (B) absorption trace (inset: NMP solution) of BPQDs, (C) spectrum, and (D) autocorrelation trace of mode-locked fiber lasers based on BPQDs. (E) Spectra and (F) autocorrelation trace of vector soliton fiber laser mode-locked by BP. (A)–(D) are reproduced with permission from Ref. [198]. Copyright 2016 Wiley-VCH Publishing. (E) and (F) are reproduced with permission from Ref. [145]. Copyright 2016 OSA Publishing.

In 2019, Zhang et al. obtained an ultrashort pulse (104 fs) in a dispersion-managed fiber laser by depositing $Ti_3C_2T_x$ onto a microfiber [189]. The spectrum and the autocorrelation trace are shown in Figure 6E and F, respectively. Wang et al. reported a high-energy pulse (~305 nJ) realized in a Q-switched fiber laser based on $Ti_3C_2T_x$ by optical deposition [188], which shows that $Ti_3C_2T_x$ could be applied as an SA for high-energy pulse generation. Yi et al. demonstrated the solution processing Ti_2CT_x operated in three different fiber lasers (1-, 1.5-, and 2.8-μm bands) [199], indicating the excellent non-linear absorption performance of Ti_2CT_x in the mid-infrared regime.

As a kind of emerging new 2DM, some MXene-based SAs possess high modulation depth, which is beneficial to obtain ultrafast pulses (~38%) [186]. Besides, MXenes can also be operated as broadband SAs from the near- to mid-infrared band [199]. It can be expected that MXene-based SAs will bring more surprises to the research and development of ultrafast photonics in lasers.

4 Perspective

The development of 2DM-based fiber lasers has brought great convenience to industry because of their compactness, flexibility, broadband operation, and high pulse quality. 2DM-based SAs are being developed rapidly and attracting substantial attention [214–217]. Graphene has excellent broadband operation and an adjustable modulation depth that depends on its layer number [33]. Graphene-based 2DMs have also been used to achieve single-frequency Q-switching [218], singly polarized

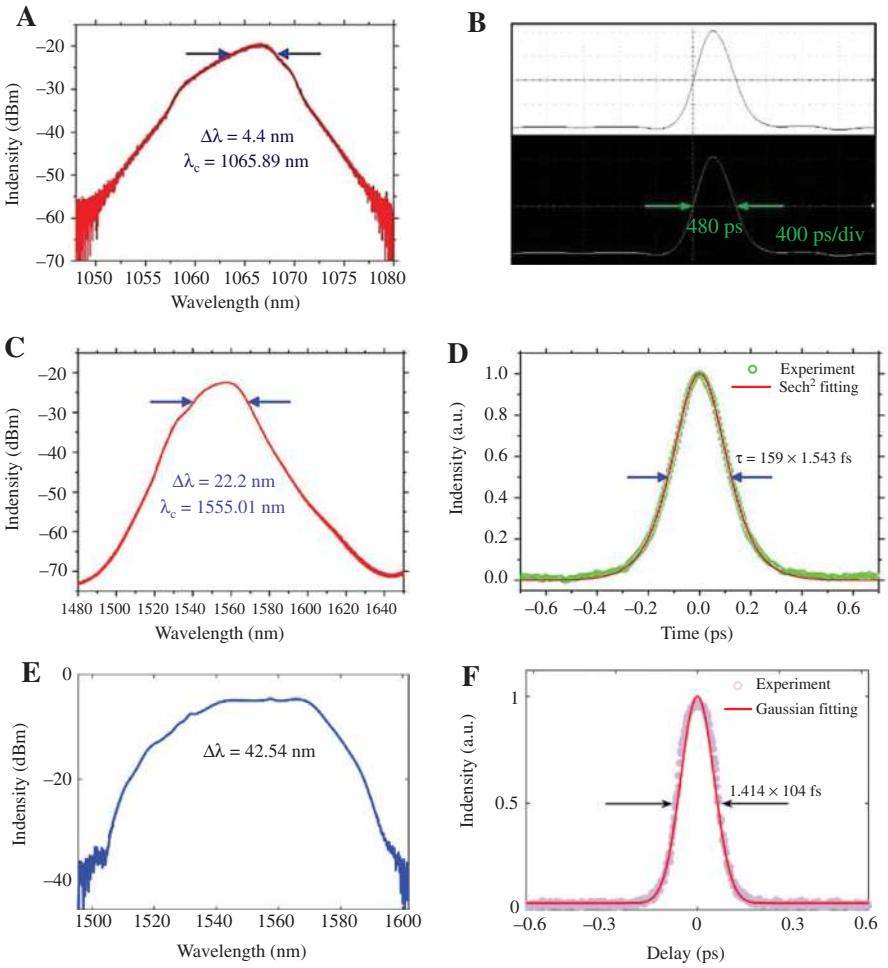

Figure 6: Mode-locked results enabled by MXene-based SAs.
(A) Spectrum and (B) pulse profile in Yb-doped fiber laser. (C) Spectrum and (D) autocorrelation trace in Er-doped fiber laser. (E) Spectrum and (F) autocorrelation trace in a dispersion-managed fiber laser. (A)–(D) are reproduced with permission from Ref. [186]. Copyright 2016 Wiley-VCH Publishing. (E) and (F) are reproduced with permission from Ref. [189]. Copyright 2019 OSA Publishing.

pulse generation [219], optical frequency comb [220], and broadband gate-tunable terahertz plasmons [221]. TIs can achieve a high modulation depth, and TMDs have better saturable absorption compared with graphene; however, the mode-locked stability of TIs and TMDs still needs to be improved. Although BP is easily oxidized in the air, it can be operated in the mid-infrared band [211]. Besides, BP as a platform of nanomedicine has also been used for biomedical diagnosis [222–224]. As a new family member of 2DMs, MXenes have many desirable properties, such as high modulation depth and broadband operation [190, 199]. However, the existing 2DM-based SAs also have their own shortcomings. In order to overcome the existing shortcomings of 2DMs and achieve wide applications in industry, some other mono-elemental 2D materials, such as antimonene and bismuthene, have attracted more attention [225–233]. In 2017, Song et al. experimentally investigated the broadband non-linear optical response of few-layer antimonene as SA, and obtained ~550-fs pulses in an Er-doped fiber laser [225]. In 2018, Lu et al. obtained 652-fs pulses in a bismuthene-based mode-locked fiber laser [226]. In addition, Ge et al. exploited few-layer selenium-doped BP nanosheets as SA to achieve mode-locked pulses in an Er-doped fiber laser, indicating that selenium-doped BP is an excellent SA candidate for ultrafast photonics [234]. To date, there have been various attempts to avoid their drawbacks. Different preparation methods have been studied to obtain SAs with better performance [235–237].

From a processing standpoint, while ultrasonication and intercalation potentially suffer from poor scalability, other exfoliation methods have been demonstrated as effective LPE techniques. These include ball milling and shear exfoliation. Ball milling is an exfoliation technique that has been demonstrated for graphene and MoS_2 [238, 239]. It uses

collisions and shear forces to disrupt the layer-to-layer interactions. Originally being an industrial process, it is intrinsically scalable. Shear exfoliation is based on the action of a rotor/stator or a rotating blade [240–243]. Exfoliation occurs by shear forces and produces large flakes of single- and few-layer material [240]. This is also a simple industrial process and thus intrinsically scalable, as it allows processing of much larger volumes than ultrasonication and higher production rates, thus reducing the potential cost. While ball milling and shear exfoliation are still batch processes, a continuous process has recently been developed for the exfoliation of graphite into graphene that uses turbulent flow and high pressure and does not require a centrifugation step afterwards [244]. Such methods, to our knowledge, have not been used thus far to produce SAs. However, they seem to be very promising methods to achieve 2DM dispersions suitable for SA fabrication at a lower cost and on a larger scale than ultrasonication or intercalation, and may thus find applications in this field in the near future.

5 Conclusion

We have reviewed solution-processed 2D materials for ultrafast fiber lasers. Exfoliation, stabilization, sorting, and MXene fabrication are introduced in this review. The applications of 2DM-based SAs such as graphene, TIs, TMDs, BP, and MXenes in ultrafast fiber lasers have been discussed. In addition, a summary and outlook has been presented in perspective. We believe that the exploration of 2DMs for ultrafast photonics will never stop, and we look forward to seeing the better combination of 2DMs and fiber lasers in the near future.

Acknowledgment: This work was supported by the National Natural Science Foundation of China (61827802 and 61961130393, Funder Id: http://dx.doi.org/10.13039/501100001809), Beijing Natural Science Foundation (4202044, Funder Id: http://dx.doi.org/10.13039/501100004826), National Key Research and Development Project (2018YFB2003200), Fundamental Research Funds for the Central Universities, Open Fund of IPOC (BUPT), and the Start-up Program of BUAA-CCMU Advanced Innovation Center for Big Data-Based Precision Medicine.

References

[1] Keller U. Recent developments in compact ultrafast lasers. Nature 2003;424:831.
[2] Fermann ME, Hartl I. Ultrafast fibre lasers. Nat Photon 2013;7:868.
[3] Song Y, Shi X, Wu C, Tang D, Zhang H. Recent progress of study on optical solitons in fiber lasers. Appl Phys Rev 2019;6:021313.
[4] Fried NM, Murray KE. High-power thulium fiber laser ablation of urinary tissues at 1.94 μm. J Endourol 2005;19:25–31.
[5] Fu B, Popa D, Zhao Z, et al. Wavelength tunable soliton rains in a nanotube-mode locked Tm-doped fiber laser. Appl Phys Lett 2018;113:193102.
[6] van Gemert MJ, Welch A. Time constants in thermal laser medicine. Lasers Surg Med 1989;9:405–21.
[7] Xie Z, Xing C, Huang W, et al. Ultrathin 2D nonlayered tellurium nanosheets: facile liquid-phase exfoliation, characterization, and photoresponse with high performance and enhanced stability. Adv Funct Mater 2018;28:1705833.
[8] Xing C, Huang W, Xie Z, et al. Ultrasmall bismuth quantum dots: facile liquid-phase exfoliation, characterization, and application in high-performance UV-Vis photodetector. ACS Photon 2018;5:621–9.
[9] Letokhov V. Laser biology and medicine. Nature 1985;316:325.
[10] Xie Z, Chen S, Duo Y, et al. Biocompatible two-dimensional titanium nanosheets for multimodal imaging-guided cancer theranostics. ACS Appl Mater Interfaces 2019;11:22129–40.
[11] Li Z, Heidt A, Simakov N, et al. Diode-pumped wideband thulium-doped fiber amplifiers for optical communications in the 1800–2050 nm window. Opt Express 2013;21:26450–5.
[12] Okhotnikov O, Grudinin A, Pessa M. Ultra-fast fibre laser systems based on SESAM technology: new horizons and applications. New J Phys 2004;6:177.
[13] Matsas V, Newson T, Zervas M. Self-starting passive mode-locked fibre ring laser exploiting non-linear polarisation switching. Opt Commun 1992;92:61–6.
[14] Alcock IP, Tropper AC, Ferguson AI, Hanna DC. Q-switched operation of a neodymium-doped monomode fibre laser. Electron Lett 1986;22:84–5.
[15] DeMaria AJ, Stetser DA, Heynau H. Self mode-locking of lasers with saturable absorbers. Appl Phys Lett 1966;8:174–6.
[16] Chen Y, Zhao C, Huang H, et al. Self-assembled topological insulator: Bi_2Se_3 membrane as a passive Q-switcher in an erbium-doped fiber laser. J Lightwave Technol 2013;31:2857–63.
[17] Li J, Luo H, Wang L, et al. 3-μm mid-infrared pulse generation using topological insulator as the saturable absorber. Opt Lett 2015;40:3659–62.
[18] Zhang H, Bao Q, Tang D, Zhao L, Loh K. Large energy soliton erbium-doped fiber laser with a graphene-polymer composite mode locker. Appl Phys Lett 2009;95:141103.
[19] Zhang M, Howe RCT, Woodward RI, et al. Solution processed MoS_2-PVA composite for sub-bandgap mode-locking of a wideband tunable ultrafast Er:fiber laser. Nano Res 2015;8:1522–34.
[20] He J, Tao L, Zhang H, Zhou B, Li J. Emerging 2D materials beyond graphene for ultrashort pulse generation in fiber lasers. Nanoscale 2019;11:2577–93.
[21] Okhotnikov O, Jouhti T, Konttinen J, Karirinne S, Pessa M. 1.5-μm monolithic GaInNAs semiconductor saturable-absorber mode locking of an erbium fiber laser. Opt Lett 2003;28:364–6.
[22] Matsas VJ, Newson TP, Richardson DJ, Payne DN. Self-starting passively mode-locked fibre ring soliton laser exploiting nonlinear polarisation rotation. Electron Lett 1992;28:1391–3.

[23] Guo B, Xiao Q, Wang S, Zhang H. 2D layered materials: synthesis, nonlinear optical properties, and device applications. Laser Photon Rev 2019;13:1800327.
[24] Xing C, Xie Z, Liang Z, et al. 2D nonlayered selenium nanosheets: facile synthesis, photoluminescence, and ultrafast photonics. Adv Opt Mater 2017;5:1700884.
[25] Fan T, Xie Z, Huang W, Li Z, Zhang H. Two-dimensional nonlayered selenium nanoflakes: facile fabrications and applications for self-powered photo-detector. Nanotechnology 2019;30:114002.
[26] Zhang B, Fan T, Xie N, Nie G, Zhang H. Versatile applications of metal single-atom @ 2D material nanoplatforms. Adv Sci 2019;6:1901787.
[27] Xie Z, Peng YP, Yu L, et al. Solar-inspired water purification based on emerging two-dimensional materials: status and challenges. Solar RRL 2019;1900400.
[28] Fang Q, Li J, Shi W, et al. 5 kW near-diffraction-limited and 8 kW high-brightness monolithic continuous wave fiber lasers directly pumped by laser diodes. IEEE Photon J 2017;9:1–7.
[29] Jiang T, Yin K, Wang C, et al. Ultrafast fiber lasers mode-locked by two-dimensional materials: review and prospect. Photon Res 2020;8:78–90.
[30] Ma C, Wang C, Gao B, Adams J, Wu G, Zhang H. Recent progress in ultrafast lasers based on 2D materials as a saturable absorber. Appl Phys Rev 2019;6:041304.
[31] Fu B, Hua Y, Xiao X, Zhu H, Sun Z, Yang C. Broadband graphene saturable absorber for pulsed fiber lasers at 1, 1.5, and 2 μm. IEEE J Select Top Quant Electron 2014;20:411–5.
[32] Wei R, Zhang H, Hu Z, et al. Ultra-broadband nonlinear saturable absorption of high-yield MoS_2 nanosheets. Nanotechnology 2016;27:305203.
[33] Bao Q, Zhang H, Wang Y, et al. Atomic-layer graphene as a saturable absorber for ultrafast pulsed lasers. Adv Funct Mater 2009;19:3077–83.
[34] Wang K, Wang J, Fan J, et al. Ultrafast saturable absorption of two-dimensional MoS_2 nanosheets. ACS Nano 2013;7:9260–7.
[35] Tian X, Wei R, Liu M, et al. Ultrafast saturable absorption in TiS_2 induced by non-equilibrium electrons and generation of femtosecond mode-locked laser. Nanoscale 2018;10:9608–15.
[36] Sun Z, Hasan T, Torrisi F, et al. Graphene mode-locked ultrafast laser. ACS Nano 2010;4:803–10.
[37] Hasan T, Sun Z, Wang F, et al. Nanotube-polymer composites for ultrafast photonics. Adv Mater 2009;21:3074–899.
[38] Zhao C, Zhang H, Qi X, Chen Y, Wang Z. Ultra-short pulse generation by a topological insulator based saturable absorber. Appl Phys Lett 2012;101:211106.
[39] Zhang M, Hu G, Hu G, et al. Yb- and Er-doped fiber laser Q-switched with an optically uniform, broadband WS_2 saturable absorber. Sci Rep 2015;5:17482.
[40] Xu J, Liu J, Wu S, Yang QH, Wang P. Graphene oxide mode-locked femtosecond erbium-doped fiber lasers. Opt Express 2012;20:15474–80.
[41] Sun Z, Popa D, Hasan T, et al. A stable, wideband tunable, near transform-limited, graphene-mode-locked, ultrafast laser. Nano Res 2010;3:653–60.
[42] Song H, Wang Q, Zhang Y, Li L. Mode-locked ytterbium-doped all-fiber lasers based on few-layer black phosphorus saturable absorbers. Opt Commun 2017;394:157–60.
[43] Tour JM. Top-down versus bottom-up fabrication of graphene-based electronics. Chem Mater 2014;26:163–71.
[44] Li X, Cai W, An J, et al. Large-area synthesis of high-quality and uniform graphene films on copper foils. Science 2009;324:1312–4.
[45] Sukang B, Hyeongkeun K, Youngbin L, et al. Roll-to-roll production of 30-inch graphene films for transparent electrodes. Nat Nanotechnol 2010;5:574–8.
[46] Hao Y, Bharathi MS, Wang L, et al. The role of surface oxygen in the growth of large single-crystal graphene on copper. Science 2013;342:720–3.
[47] Fiori G, Bonaccorso F, Iannaccone G, et al. Electronics based on two-dimensional materials. Nat Nanotechnol 2014;9:768–79.
[48] Wang QH, Kalantar-Zadeh K, Kis A, Coleman JN, Strano MS. Electronics and optoelectronics of two-dimensional transition metal dichalcogenides. Nat Nanotechnol 2012;7:699–712.
[49] Bonaccorso F, Colombo L, Yu G, et al. Graphene, related two-dimensional crystals, and hybrid systems for energy conversion and storage. Science 2015;347:1246501.
[50] Zhi C, Bando Y, Tang C, Kuwahara H, Golberg D. Large-scale fabrication of boron nitride nanosheets and their utilization in polymeric composites with improved thermal and mechanical properties. Adv Mater 2009;21:2889–93.
[51] Yao B, Yu C, Wu Y, et al. Graphene-enhanced Brillouin optomechanical microresonator for ultrasensitive gas detection. Nano Lett 2017;17:4996–5002.
[52] Cao Z, Yao B, Qin C, et al. Biochemical sensing in graphene-enhanced microfiber resonators with individual molecule sensitivity and selectivity. Light Sci Appl 2019;8:1–10.
[53] Nicolosi V, Chhowalla M, Kanatzidis MG, Strano MS, Coleman JN. Liquid exfoliation of layered materials. Science 2013;340:1226419.
[54] Bonaccorso F, Lombardo A, Hasan T, Sun Z, Colombo L, Ferrari AC. Production and processing of graphene and 2D crystals. Mater Today 2012;15:564–89.
[55] Bonaccorso F, Bartolotta A, Coleman JN, Backes C. 2D-crystal-based functional inks. Adv Mater 2016;28:6136–66.
[56] Niu L, Coleman JN, Zhang H, Shin H, Chhowalla M, Zheng Z. Production of two-dimensional nanomaterials via liquid-based direct exfoliation. Small 2016;12:272–93.
[57] Hummers WS, Offeman RE. Preparation of graphitic oxide. J Am Chem Soc 1958;80:1339.
[58] Dreyer DR, Park S, Bielawski CW, Ruoff RS. The chemistry of graphene oxide. Chem Soc Rev 2010;39:228–40.
[59] Sun L, Lin Z, Peng J, Weng J, Huang Y, Luo Z. Preparation of few-layer bismuth selenide by liquid-phase-exfoliation and its optical absorption properties. Sci Rep 2014;4:4794.
[60] Woodward RI, Howe RCT, Runcorn TH, et al. Wideband saturable absorption in few-layer molybdenum diselenide ($MoSe_2$) for Q-switching Yb-, Er- and Tm-doped fiber lasers. Opt Express 2015;23:20051–61.
[61] Hasan T, Torrisi F, Sun Z, et al. Solution-phase exfoliation of graphite for ultrafast photonics. Phys Status Sol 2010;247:2953–7.
[62] Liu J, Wu S, Yang QH, Wang P. Stable nanosecond pulse generation from a graphene-based passively Q-switched Yb-doped fiber laser. Opt Lett 2011;36:4008–10.
[63] Popa D, Sun Z, Torrisi F, Hasan T, Wang F, Ferrari AC. Sub 200 fs pulse generation from a graphene mode-locked fiber laser. Appl Phys Lett 2010;97:203106.
[64] Popa D, Sun Z, Hasan T, Torrisi F, Wang F, Ferrari AC. Graphene Q-switched, tunable fiber laser. Appl Phys Lett 2011;98:073106.

[65] Purdie DG, Popa D, Wittwer VJ, et al. Few-cycle pulses from a graphene mode-locked all-fiber laser. Appl Phys Lett 2015;106:253101.
[66] Zhang M, Kelleher EJR, Torrisi F, et al. Tm-doped fiber laser mode-locked by graphene-polymer composite. Opt Express 2012;20:25077–84.
[67] Torrisi F, Popa D, Milana S, et al. Stable, surfactant-free graphene-styrene methylmethacrylate composite for ultrafast lasers. Adv Opt Mater 2016;4:1088–97.
[68] Lin YH, Yang CY, Liou JH, Yu CP, Lin GR. Using graphene nanoparticle embedded in photonic crystal fiber for evanescent wave mode-locking of fiber laser. Opt Express 2013;21:16763–76.
[69] Bao Q, Zhang H, Yang JX, et al. Graphene-polymer nanofiber membrane for ultrafast photonics. Adv Funct Mater 2010;20:782–91.
[70] Li X, Wang Y, Wang Y, et al. All-normal-dispersion passively mode-locked Yb-doped fiber ring laser based on a graphene oxide saturable absorber. Laser Phys Lett 2013;10:075108.
[71] Zhao J, Wang Y, Yan P, et al. An L-band graphene-oxide mode-locked fiber laser delivering bright and dark pulses. Laser Phys 2013;23:075105.
[72] Zhao J, Wang Y, Yan P, et al. An ytterbium-doped fiber laser with dark and Q-switched pulse generation using graphene-oxide as saturable absorber. Opt Commun 2014;312:227–32.
[73] Liu ZB, He X, Wang DN. Passively mode-locked fiber laser based on a hollow-core photonic crystal fiber filled with few-layered graphene oxide solution. Opt Lett 2011;36:3024–6.
[74] Jung M, Koo J, Park J, et al. Mode-locked pulse generation from an all-fiberized, Tm-Ho-codoped fiber laser incorporating a graphene oxide-deposited side-polished fiber. Opt Express 2013;21:20062–72.
[75] Jung M, Koo J, Debnath P, Song YW, Lee JH. A mode-locked 1.91 μm fiber laser based on interaction between graphene oxide and evanescent field. Appl Phys Exp 2012;5:112702.
[76] Lee J, Koo J, Debnath P, Song YW, Lee JH. A Q-switched, mode-locked fiber laser using a graphene oxide-based polarization sensitive saturable absorber. Laser Phys Lett 2013;10:035103.
[77] Gui L, Zhang W, Li X, et al. Self-assembled graphene membrane as an ultrafast mode-locker in an erbium fiber laser. IEEE Photon Technol Lett 2011;23:1790–2.
[78] Wang J, Luo Z, Zhou M, et al. Evanescent-light deposition of graphene onto tapered fibers for passive Q-switch and mode-locker. IEEE Photon J 2012;4:1295–305.
[79] Wang Z, Chen Y, Zhao C, Zhang H, Wen S. Switchable dual-wavelength synchronously Q-switched erbium-doped fiber laser based on graphene saturable absorber. IEEE Photon J 2012;4:869–76.
[80] Fu B, Gui L, Zhang W, Xiao X, Zhu H, Yang C. Passive harmonic mode locking in erbium-doped fiber laser with graphene saturable absorber. Opt Commun 2013;286:304–8.
[81] Fu B, Li J, Cao Z, Popa D. Bound states of solitons in a harmonic graphene-mode-locked fiber laser. Photon Res 2019;7:116.
[82] Sobon G, Sotor J, Jagiello J, et al. Graphene oxide vs reduced graphene oxide as saturable absorbers for Er-doped passively mode-locked fiber laser. Opt Express 2012;20:19463.
[83] Woodward RI, Kelleher EJR, Howe RCT, et al. Tunable Q-switched fiber laser based on saturable edge-state absorption in few-layer molybdenum disulfide (MoS_2). Opt Express 2014;22:31113–22.
[84] Chen B, Zhang X, Wu K, Wang H, Wang J, Chen J. Q-switched fiber laser based on transition metal dichalcogenides MoS_2, $MoSe_2$, WS_2, and WSe_2. Opt Express 2015;23:26723–37.
[85] Huang Y, Luo Z, Li Y, et al. Widely-tunable, passively Q-switched erbium-doped fiber laser with few-layer MoS_2 saturable absorber. Opt Express 2014;22:25258–66.
[86] Ahmed MHM, Latiff A, Arof H, Ahmad H, Harun SW. Femtosecond mode-locked erbium-doped fiber laser based on MoS_2-PVA saturable absorber. Opt Laser Technol 2016;82:145–9.
[87] Luo Z, Huang Y, Min Z, et al. 1-, 1.5-, and 2-μm fiber lasers Q-switched by a broadband few-layer MoS_2 saturable absorber. J Lightwave Technol 2014;32:4077–84.
[88] Li W, Peng J, Zhong Y, et al. Orange-light passively Q-switched Pr^{3+}-doped all-fiber lasers with transition-metal dichalcogenide saturable absorbers. Opt Mater Exp 2016;6:2031–9.
[89] Liu H, Zheng X, Liu M, et al. Femtosecond pulse generation from a topological insulator mode-locked fiber laser. Opt Express 2014;22:6868–73.
[90] Zhang H, Lu S, Zheng J, et al. Molybdenum disulfide (MoS_2) as a broadband saturable absorber for ultra-fast photonics. Opt Express 2014;22:7249–60.
[91] Wang J, Li S, Xing Y, Chen L, Wei Z, Wang Y. High energy passively Q-switched Yb-doped fiber laser based on WS_2 and Bi_2Te_3 saturable absorbers. J Opt 2018;8:324–31.
[92] Wu K, Zhang X, Wang J, Li X, Chen J. WS_2 as a saturable absorber for ultrafast photonic applications of mode-locked and Q-switched lasers. Opt Express 2015;23:11453–61.
[93] Du J, Wang Q, Jiang G, et al. Ytterbium-doped fiber laser passively mode locked by few-layer molybdenum disulfide (MoS_2) saturable absorber functioned with evanescent field interaction. Sci Rep 2014;4:6346.
[94] Kassani SH, Khazaeinezhad R, Jeong H, Nazari T, Yeom DI, Oh K. All-fiber Er-doped Q-switched laser based on tungsten disulfide saturable absorber. Opt Mater Express 2015;5:373–9.
[95] Lin J, Yan K, Zhou Y, Xu LX, Gu C, Zhan QW. Tungsten disulphide based all fiber Q-switching cylindrical-vector beam generation. Appl Phys Lett 2015;107:191108.
[96] Mao D, She X, Du B, et al. Erbium-doped fiber laser passively mode locked with few-layer $WSe_2/MoSe_2$ nanosheets. Sci Rep 2016;6:23583.
[97] Mao D, Wang Y, Ma C, et al. WS_2 mode-locked ultrafast fiber laser. Sci Rep 2015;5:7965.
[98] Liu M, Zheng X, Qi Y, et al. Microfiber-based few-layer MoS_2 saturable absorber for 2.5 GHz passively harmonic mode-locked fiber laser. Opt Express 2014;22:22841–6.
[99] Chen B, Zhang X, Guo C, Wu K, Chen J, Wang J. Tungsten diselenide Q-switched erbium-doped fiber laser. Opt Eng 2016;55:801306.
[100] Zhu X, Chen S, Zhang M, et al. TiS_2-based saturable absorber for ultrafast fiber lasers. Photon Res 2018;6:50–4.
[101] Li J, Zhao Y, Chen Q, Niu K, Sun R, Zhang H. Passively mode-locked ytterbium-doped fiber laser based on SnS_2 as saturable absorber. IEEE Photon J 2017;9:1–7.
[102] Niu K, Sun R, Chen Q, Man B, Zhang H. Passively mode-locked Er-doped fiber laser based on SnS_2 nanosheets as a saturable absorber. Photon Res 2018;6:72–6.
[103] Mao D, Cui X, Gan X, et al. Passively Q-switched and mode-locked fiber laser based on a ReS_2 saturable absorber. IEEE J Select Top Quant Electron 2017;24:1100406.
[104] Cheng PK, Tang CY, Wang XY, Ma S, Long H, Tsang YH. Passively Q-switched ytterbium doped fiber laser based on

broadband multilayer platinum ditelluride ($PtTe_2$) saturable absorber. Sci Rep 2019;9:1–7.
[105] Wu D, Cai Z, Zhong Y, et al. 635 nm visible Pr^{3+}-doped ZBLAN fiber lasers Q-switched by topological insulators SAs. IEEE Photon Technol Lett 2015;27:2379–82.
[106] Yan P, Lin R, Zhang H, Liu A, Yang H, Ruan S. Topological insulator solution filled in photonic crystal fiber for passive mode-locked fiber laser. IEEE Photon Technol Lett 2015;27:264–7.
[107] Li W, Zou J, Huang Y, et al. 212-kHz-linewidth, transform-limited pulses from a single-frequency Q-switched fiber laser based on a few-layer Bi_2Se_3 saturable absorber. Photon Res 2018;6:C29–35.
[108] Guo B, Yao Y, Yang Y, et al. Topological insulator: Bi_2Se_3/polyvinyl alcohol film-assisted multi-wavelength ultrafast erbium-doped fiber laser. J Appl Phys 2015;117:063108.
[109] Lin H, Li W, Lan J, Guan X, Xu H, Cai Z. All-fiber passively Q-switched 604 nm praseodymium laser with a Bi_2Se_3 saturable absorber. Appl Opt 2017;56:802–5.
[110] Zhao C, Zou Y, Chen Y, et al. Wavelength-tunable picosecond soliton fiber laser with topological insulator: Bi_2Se_3 as a mode locker: erratum. Opt Express 2013;20:27888–95.
[111] Dou Z, Song Y, Tian J, Liu J, Yu Z, Fang X. Mode-locked ytterbium-doped fiber laser based on topological insulator: Bi_2Se_3. Opt Express 2014;22:24055.
[112] Meng Y, Semaan G, Salhi M, et al. High power L-band mode-locked fiber laser based on topological insulator saturable absorber. Opt Express 2015;23:23053–8.
[113] Gao L, Huang W, Zhang J, et al. Q-switched mode-locked erbium-doped fiber laser based on topological insulator Bi_2Se_3 deposited fiber taper. Appl Opt 2014;53:5117–22.
[114] Gao L, Zhu T, Huang W, Luo Z. Stable, ultrafast pulse mode-locked by topological insulator Bi_2Se_3 nanosheets interacting with photonic crystal fiber: from anomalous dispersion to normal dispersion. IEEE Photon J 2015;7:1–8.
[115] Boguslawski J, Sotor J, Sobon G, et al. Mode-locked Er-doped fiber laser based on liquid phase exfoliated Sb_2Te_3 topological insulator. Laser Phys 2014;24:105111.
[116] Li J, Luo H, Zhai B, et al. Black phosphorus: a two-dimension saturable absorption material for mid-infrared Q-switched and mode-locked fiber lasers. Sci Rep 2016;6:30361.
[117] Qin Z, Xie G, Zhang H, et al. Black phosphorus as saturable absorber for the Q-switched Er:ZBLAN fiber laser at 28 μm. Opt Express 2015;23:24713–8.
[118] Chen Y, Chen S, Liu J, Gao Y, Zhang W. Sub-300 femtosecond soliton tunable fiber laser with all-anomalous dispersion passively mode locked by black phosphorus. Opt Express 2016;24:13316–24.
[119] Du J, Zhang M, Guo Z, et al. Phosphorene quantum dot saturable absorbers for ultrafast fiber lasers. Sci Rep 2017;7:42357.
[120] Liu M, Jiang X, Yan Y, et al. Black phosphorus quantum dots for femtosecond laser photonics. Opt Commun 2018;406:85–90.
[121] Liu J, Zhao F, Wang H, et al. Generation of dark solitons in erbium-doped fiber laser based on black phosphorus nanoparticles. Opt Mater 2019;89:100–5.
[122] Yu H, Zheng X, Yin K, Cheng X, Jiang T. Thulium/holmium-doped fiber laser passively mode locked by black phosphorus nanoplatelets-based saturable absorber. Appl Opt 2015;54:10290–4.
[123] Yu H, Zheng X, Yin K, Cheng X, Jiang T. Nanosecond passively Q-switched thulium/holmium-doped fiber laser based on black phosphorus nanoplatelets. Opt Mater Express 2016;6:603–9.
[124] Luo Z, Liu M, Guo Z, et al. Microfiber-based few-layer black phosphorus saturable absorber for ultra-fast fiber laser. Opt Express 2015;23:20030–9.
[125] Mao D, Li M, Cui X, et al. Stable high-power saturable absorber based on polymer-black-phosphorus films. Opt Commun 2018;406:254–9.
[126] Wu D, Cai Z, Zhong Y, et al. Compact passive Q-switching Pr^{3+}-doped ZBLAN fiber laser with black phosphorus-based saturable absorber. IEEE J Select Top Quant Electron 2016;23:7–12.
[127] Zhao R, He J, Su X, et al. Tunable high-power Q-switched fiber laser based on BP-PVA saturable absorber. IEEE J Select Top Quant Electron 2017;24:1–5.
[128] Yun L. Black phosphorus saturable absorber for dual-wavelength polarization-locked vector soliton generation. Opt Express 2017;25:32380–5.
[129] Jin X, Hu G, Zhang M, et al. 102 fs pulse generation from a long-term stable, inkjet-printed black phosphorus-mode-locked fiber laser. Opt Express 2018;26:12506–13.
[130] Liu H, Song W, Yu Y, Jiang Q, Pang F, Wang T. Black phosphorus-film with drop-casting method for high-energy pulse generation from Q-switched Er-doped fiber laser. Photon Sensors 2019;9:239–45.
[131] Wang T, Zhang W, Shi X, et al. Black phosphorus-enabled harmonic mode locking of dark pulses in a Yb-doped fiber laser. Laser Phys Lett 2019;16:085102.
[132] Wang T, Jin X, Yang J, et al. Ultra-stable pulse generation in ytterbium-doped fiber laser based on black phosphorus. Nanoscale Adv 2019;1:195–202.
[133] Hernandez Y, Nicolosi V, Lotya M, et al. High-yield production of graphene by liquid-phase exfoliation of graphite. Nat Nanotechnol 2008;3:563–8.
[134] Lotya M, Hernandez Y, King PJ, et al. Liquid phase production of graphene by exfoliation of graphite in surfactant/water solutions. J Am Chem Soc 2009;131:3611–20.
[135] Coleman JN, Lotya M, O'Neill A, et al. Two-dimensional nanosheets produced by liquid exfoliation of layered materials. Science 2011;331:568–71.
[136] Luo Z, Huang Y, Weng J, et al. 1.06 μm Q-switched ytterbium-doped fiber laser using few-layer topological insulator Bi_2Se_3 as a saturable absorber. Opt Express 2013;21:29516–22.
[137] Li K, Song Y, Yu Z, Xu R, Dou Z, Tian J. L-band femtosecond fibre laser based on Bi_2Se_3 topological insulator. Laser Phys Lett 2015;12:105103.
[138] Lin JH, Huang GH, Ou CH, et al. Q-switched pulse and mode-locked pulse generation from a Yb^{3+}-doped fiber laser based on Bi_2Se_3. IEEE Photon J 2018;10:1–10.
[139] Wang Y, Mao D, Gan X, et al. Harmonic mode locking of bound-state solitons fiber laser based on MoS_2 saturable absorber. Opt Express 2015;23:205.
[140] Khazaeinezhad R, Kassani SH, Jeong H, et al. Ultrafast pulsed all-fiber laser based on tapered fiber enclosed by few-layer WS_2 nanosheets. IEEE Photon Technol Lett 2015;27:1581–4.
[141] Lee J, Koo J, Lee J, Jhon YM, Lee JH. All-fiberized, femtosecond laser at 1912 nm using a bulk-like $MoSe_2$ saturable absorber. Opt Mater Express 2017;7:2968–79.
[142] Koo J, Park J, Lee J, Jhon YM, Lee JH. Femtosecond harmonic mode-locking of a fiber laser at 3.27 GHz using a bulk-like, $MoSe_2$-based saturable absorber. Opt Express 2016;24:10575–89.
[143] Hanlon D, Backes C, Doherty E, et al. Liquid exfoliation of solvent-stabilized few-layer black phosphorus for applications beyond electronics. Nat Commun 2015;6:8563.

[144] Pawliszewska M, Ge Y, Li Z, Zhang H, Sotor J. Fundamental and harmonic mode-locking at 21 μm with black phosphorus saturable absorber. Opt Express 2017;25:16916–21.
[145] Song Y, Chen S, Zhang Q, et al. Vector soliton fiber laser passively mode locked by few layer black phosphorus-based optical saturable absorber. Opt Express 2016;24:25933–42.
[146] Coleman JN. Liquid exfoliation of defect-free graphene. Acc Chem Res 2012;46:14–22.
[147] Ciesielski A, Samori P. Graphene via sonication assisted liquid-phase exfoliation. Chem Soc Rev 2014;43:381–98.
[148] Chen S, Zhao C, Li Y, et al. Broadband optical and microwave nonlinear response in topological insulator. Opt Mater Express 2014;4:587–96.
[149] Chen Y, Wu M, Tang P, et al. The formation of various multi-soliton patterns and noise-like pulse in a fiber laser passively mode-locked by a topological insulator based saturable absorber. Laser Phys Lett 2014;11:055101.
[150] Liu J, Li X, Zhang S, et al. Polarization domain wall pulses in a microfiber-based topological insulator fiber laser. Sci Rep 2016;6:29128.
[151] Mao D, Jiang B, Gan X, et al. Soliton fiber laser mode locked with two types of film-based Bi_2Te_3 saturable absorbers. Photon Res 2015;3:A43–6.
[152] Luo ZC, Liu M, Liu H, et al. 2 GHz passively harmonic mode-locked fiber laser by a microfiber-based topological insulator saturable absorber. Opt Lett 2013;38:5212–5.
[153] Chen Y, Zhao C, Chen S, et al. Large energy, wavelength widely tunable, topological insulator Q-switched erbium-doped fiber laser. IEEE J Select Top Quant Electron 2013;20:315–22.
[154] Liu M, Zhao N, Liu H, et al. Dual-wavelength harmonically mode-locked fiber laser with topological insulator saturable absorber. Photon Technol Lett IEEE 2014;26:983–6.
[155] Jin L, Ma X, Zhang H, Zhang H, Chen H, Xu Y. 3 GHz passively harmonic mode-locked Er-doped fiber laser by evanescent field-based nano-sheets topological insulator. Opt Express 2018;26:31244–52.
[156] Joensen P, Frindt RF, Morrison SR. Single-layer MoS_2. Mater Res Bull 1986;21:457–61.
[157] Bissessur R, Kanatzidis MG, Schindler JL, Kannewurf CR. Encapsulation of polymers into MoS_2 and metal to insulator transition in metastable MoS_2. J Chem Soc Chem Commun 1993:1582–5.
[158] Zheng J, Zhang H, Dong S, et al. High yield exfoliation of two-dimensional chalcogenides using sodium naphthalenide. Nat Commun 2014;5:2995.
[159] Su CY, Lu AY, Xu Y, Chen FR, Khlobystov AN, Li LJ. High-quality thin graphene films from fast electrochemical exfoliation. ACS Nano 2011;5:2332–9.
[160] Parvez K, Li R, Puniredd SR, et al. Electrochemically exfoliated graphene as solution-processable, highly conductive electrodes for organic electronics. ACS Nano 2013;7:3598–606.
[161] Parvez K, Wu ZS, Li R, et al. Exfoliation of graphite into graphene in aqueous solutions of inorganic salts. J Am Chem Soc 2014;136:6083–91.
[162] Kim H, Cho J, Jang SY, Song YW. Deformation-immunized optical deposition of graphene for ultrafast pulsed lasers. Appl Phys Lett 2011;98:021104.
[163] Stankovich S, Dikin DA, Piner RD, et al. Synthesis of graphene-based nanosheets via chemical reduction of exfoliated graphite oxide. Carbon 2007;45:1558–65.
[164] O'Neill A, Khan U, Coleman JN. Preparation of high concentration dispersions of exfoliated MoS_2 with increased flake size. Chem Mater 2012;24:2414–21.
[165] Brent JR, Savjani N, Lewis EA, Haigh SJ, Lewis DJ, O'Brien P. Production of few-layer phosphorene by liquid exfoliation of black phosphorus. Chem Commun 2014;50:1338–41.
[166] Kang J, Wood JD, Wells SA, et al. Solvent exfoliation of electronic-grade, two-dimensional black phosphorus. ACS Nano 2015;9:3596–604.
[167] Yasaei P, Kumar B, Foroozan T, et al. High-quality black phosphorus atomic layers by liquid-phase exfoliation. Adv Mater 2015;27:1887–92.
[168] Hamilton CE, Lomeda JR, Sun Z, Tour JM, Barron AR. High-yield organic dispersions of unfunctionalized graphene. Nano Lett 2009;9:3460–2.
[169] Bourlinos AB, Georgakilas V, Zboril R, Steriotis TA, Stubos AK. Liquid-phase exfoliation of graphite towards solubilized graphenes. Small 2009;5:1841–5.
[170] Hanlon D, Backes C, Higgins TM, et al. Production of molybdenum trioxide nanosheets by liquid exfoliation and their application in high-performance supercapacitors. Chem Mater 2014;26:1751–63.
[171] Harvey A, Backes C, Gholamvand Z, et al. Preparation of gallium sulfide nanosheets by liquid exfoliation and their application as hydrogen evolution catalysts. Chem Mater 2015;27:3483–93.
[172] O'Neill A, Khan U, Nirmalraj PN, Boland J, Coleman JN. Graphene dispersion and exfoliation in low boiling point solvents. J Phys Chem C 2011;115:5422–8.
[173] Choi EY, Choi WS, Lee YB, Noh YY. Production of graphene by exfoliation of graphite in a volatile organic solvent. Nanotechnology 2011;22:365601.
[174] Qian W, Hao R, Hou Y, et al. Solvothermal-assisted exfoliation process to produce graphene with high yield and high quality. Nano Res 2009;2:706–12.
[175] Lotya M, King PJ, Khan U, De S, Coleman JN. High-concentration, surfactant-stabilized graphene dispersions. ACS Nano 2010;4:3155–62.
[176] Vadukumpully S, Paul J, Valiyaveettil S. Cationic surfactant mediated exfoliation of graphite into graphene flakes. Carbon 2009;47:3288–94.
[177] Hao R, Qian W, Zhang L, Hou Y. Aqueous dispersions of TCNQ-anion-stabilized graphene sheets. Chem Commun 2008;6576.
[178] Smith RJ, King PJ, Lotya M, et al. Large-scale exfoliation of inorganic layered compounds in aqueous surfactant solutions. Adv Mater 2011;23:3944–8.
[179] De S, King PJ, Lotya M, et al. Flexible, transparent, conducting films of randomly stacked graphene from surfactant-stabilized, oxide-free graphene dispersions. Small 2010;6:458–64.
[180] May P, Khan U, Hughes JM, Coleman JN. Role of solubility parameters in understanding the steric stabilization of exfoliated two-dimensional nanosheets by adsorbed polymers. J Phys Chem C 2012;116:11393–400.
[181] Kang J, Seo J-WT, Alducin D, Ponce A, Yacaman MJ, Hersam MC. Thickness sorting of two-dimensional transition metal dichalcogenides via copolymer-assisted density gradient ultracentrifugation. Nat Commun 2014;5:5478.
[182] Green AA, Hersam MC. Solution phase production of graphene with controlled thickness via density differentiation. Nano Lett 2009;9:4031–6.

[183] Kang J, Sangwan VK, Wood JD, et al. Layer-by-layer sorting of rhenium disulfide via high-density isopycnic density gradient ultracentrifugation. Nano Lett 2016;16:7216–23.
[184] Backes C, Szydłowska BM, Harvey A, et al. Production of highly monolayer enriched dispersions of liquid-exfoliated nanosheets by liquid cascade centrifugation. ACS Nano 2016;10:1589–601.
[185] Naguib M, Mashtalir O, Carle J, et al. Two-dimensional transition metal carbides. ACS Nano 2012;6:1322–31.
[186] Jiang X, Liu S, Liang W, et al. Broadband nonlinear photonics in few-layer MXene $Ti_3C_2T_x$ (T=F, O, or OH). Laser Photon Rev 2018;12:1700229–38.
[187] Naguib M, Kurtoglu M, Presser V, et al. Two-dimensional nanocrystals produced by exfoliation of Ti_3AlC_2. Adv Mater 2011;23:4248–53.
[188] Wang L, Li X, Wang C, et al. Few-layer MXene $Ti_3C_2T_x$ (T=F, O, or OH) for robust pulse generation in a compact Er-doped fiber laser. ChemNanoMat 2019;5:1233–8.
[189] Wu Q, Jin X, Chen S, et al. MXene-based saturable absorber for femtosecond mode-locked fiber lasers. Opt Express 2019;27:10159–70.
[190] Jhon YI, Koo J, Anasori B, et al. Metallic MXene saturable absorber for femtosecond mode-locked lasers. Adv Mater 2017;29:1702496–503.
[191] Meng S, Kong T, Ma W, Wang H, Zhang H. 2D crystal-based fibers: status and challenges. Small 2019;15:1902691.
[192] Xu J, Wu S, Li H, et al. Dissipative soliton generation from a graphene oxide mode-locked Er-doped fiber laser. Opt Express 2012;20:23653–8.
[193] Luo Z, Liu C, Huang Y, et al. Topological-insulator passively Q-switched double-clad fiber laser at 2 μm wavelength. IEEE J Select Top Quant Electron 2014;20:902708.
[194] Liu H, Luo A, Wang F, et al. Femtosecond pulse erbium-doped fiber laser by a few-layer MoS_2 saturable absorber. Opt Lett 2014;39:4591–4.
[195] Jung M, Lee J, Park J, Koo J, Jhon YM, Lee JH. Mode-locked, 1.94-μm, all-fiberized laser using WS_2-based evanescent field interaction. Opt Express 2015;23:19996–20006.
[196] Li L, Jiang S, Wang Y, et al. WS_2/fluorine mica (FM) saturable absorbers for all-normal-dispersion mode-locked fiber laser. Opt Express 2015;23:28698–706.
[197] Zhang S, Zhang X, Wang H, et al. Size-dependent saturable absorption and mode-locking of dispersed black phosphorus nanosheets. Opt Mater Express 2016;6:3159–68.
[198] Xu Y, Wang Z, Guo Z, et al. Solvothermal synthesis and ultrafast photonics of black phosphorus quantum dots. Adv Opt Mater 2016;4:1223–9.
[199] Yi J, Du L, Li J, et al. Unleashing the potential of Ti_2Ct_x MXene as a pulse modulator for mid-infrared fiber lasers. 2D Mater 2019;6:045038.
[200] Loh KP, Bao Q, Eda G, Chhowalla M. Graphene oxide as a chemically tunable platform for optical applications. Nat Chem 2010;2:1015–24.
[201] Bonaccorso F, Sun Z, Hasan T, Ferrari AC, et al. Graphene photonics and optoelectronics. Nat Photon 2010;4:611–22.
[202] Zhang H, Liu CX, Qi XL, Dai X, Fang Z, Zhang SC. Topological insulators in Bi_2Se_3, Bi_2Te_3 and Sb_2Te_3 with a single Dirac cone on the surface. Nat Phys 2009;5:438–42.
[203] Yan P, Lin R, Ruan S, et al. A practical topological insulator saturable absorber for mode-locked fiber laser. Sci Rep 2015;5:8690.
[204] Luo Z, Wu D, Xu B, et al. Two-dimensional material-based saturable absorbers: towards compact visible-wavelength all-fiber pulsed lasers. Nanoscale 2016;8:1066–72.
[205] Li S, Yin Y, Ouyang Q, et al. Dissipative soliton generation in Er-doped fibre laser using SnS_2 as a saturable absorber. Appl Phys Express 2019;12:102008.
[206] Churchill HOH, Jarillo-Herrero P. Two-dimensional crystals: phosphorus joins the family. Nat Nanotechnol 2014;9:330–1.
[207] Guo Z, Zhang H, Lu S, et al. From black phosphorus to phosphorene: basic solvent exfoliation, evolution of Raman scattering, and applications to ultrafast photonics. Adv Funct Mater 2015;25:6996–7002.
[208] Lu S, Miao L, Guo Z, et al. Broadband nonlinear optical response in multi-layer black phosphorus: an emerging infrared and mid-infrared optical material. Opt Express 2015;23:11183.
[209] Chen Y, Jiang G, Chen S, et al. Mechanically exfoliated black phosphorus as a new saturable absorber for both Q-switching and mode-locking laser operation. Opt Express 2015;23:12823.
[210] Wang D, Song H, Long X, Li L. Switchable and tunable multi-wavelength emissions in pulsed ytterbium fiber lasers with black phosphorus saturable absorbers and polarization-maintaining fiber Bragg gratings. Opt Commun 2019;452:373–9.
[211] Hu G, Albrow-Owen T, Jin X, et al. Black phosphorus ink formulation for inkjet printing of optoelectronics and photonics. Nat Commun 2017;8:278.
[212] Naguib M, Mochalin VN, Barsoum MW, Gogotsi Y. 25th Anniversary article: MXenes: a new family of two-dimensional materials. Adv Mater 2014;26:992–1005.
[213] Zhang X, Zhao X, Wu D, Jing Y, Zhou Z. High and anisotropic carrier mobility in experimentally possible Ti_2Co_2 (MXene) monolayers and nanoribbons. Nanoscale 2015;7:16020–5.
[214] Zhang Y, Lim CK, Dai Z, et al. Photonics and optoelectronics using nano-structured hybrid perovskite media and their optical cavities. Phys Rep 2019;795:1–51.
[215] Guo S, Zhang Y, Ge Y, Zhang S, Zeng H, Zhang H. 2D V-V binary materials: status and challenges. Adv Mater 2019;31:1902352.
[216] Zhang Y, Liu J, Wang Z, et al. Synthesis, properties, and optical applications of low-dimensional perovskites. Chem Commun 2016;52:13637–55.
[217] Li P, Chen Y, Yang T, et al. Two-dimensional $CH_3NH_3PBi_3$ perovskite nanosheets for ultrafast pulsed fiber lasers. ACS Appl Mater Interfaces 2017;9:12759–65.
[218] Yao B, Rao Y, Huang S, et al. Graphene Q-switched distributed feedback fiber lasers with narrow linewidth approaching the transform limit. Opt Express 2017;25:8202–11.
[219] Yao B, Rao Y, Wang Z, et al. Graphene based widely-tunable and singly-polarized pulse generation with random fiber lasers. Sci Rep 2015;5:18526.
[220] Yao B, Huang SW, Liu Y, et al. Gate-tunable frequency combs in graphene-nitride microresonators. Nature 2018;558:410–4.
[221] Yao B, Liu Y, Huang SW, et al. Broadband gate-tunable terahertz plasmons in graphene heterostructures. Nat Photon 2018;12:22–8.
[222] Fan T, Zhou Y, Qiu M, Zhang H. Black phosphorus: a novel nanoplatform with potential in the field of bio-photonic nanomedicine. J Innov Opt Health Sci 2018;11:1830003.

[223] Luo M, Fan T, Zhou Y, Zhang H, Mei L. 2D black phosphorus-based biomedical applications. Adv Funct Mater 2019;29:1808306.
[224] Xie Z, Wang D, Fan T, et al. Black phosphorus analogue tin sulfide nanosheets: synthesis and application as near-infrared photothermal agents and drug delivery platforms for cancer therapy. J Mater Chem B 2018;6:4747–55.
[225] Song Y, Liang Z, Jiang X, et al. Few-layer antimonene decorated microfiber: ultra-short pulse generation and all-optical thresholding with enhanced long term stability. 2D Mater 2017;4:045010.
[226] Lu L, Liang Z, Wu L, et al. Few-layer bismuthene: sonochemical exfoliation, nonlinear optics and applications for ultrafast photonics with enhanced stability. Laser Photon Rev 2018;12:1700221.
[227] Song Y, You K, Chen Y, et al. Lead monoxide: a promising two-dimensional layered material for applications in nonlinear photonics in the infrared band. Nanoscale 2019;11:12595–602.
[228] Luo H, Tian X, Gao Y, et al. Antimonene: a long-term stable two-dimensional saturable absorption material under ambient conditions for the mid-infrared spectral region. Photon Res 2018;6:900–7.
[229] Liu G, Zhang F, Wu T, et al. Single-and dual-wavelength passively mode-locked erbium-doped fiber laser based on antimonene saturable absorber. IEEE Photon J 2019;11:1–11.
[230] Chai T, Li X, Feng T, et al. Few-layer bismuthene for ultrashort pulse generation in a dissipative system based on an evanescent field. Nanoscale 2018;10:17617–22.
[231] Yang Q, Liu R, Huang C, et al. 2D bismuthene fabricated via acid-intercalated exfoliation showing strong nonlinear near-infrared responses for mode-locking lasers. Nanoscale 2018;10:21106–15.
[232] Guo B, Wang S, Wu Z, et al. Sub-200 fs soliton mode-locked fiber laser based on bismuthene saturable absorber. Opt Express 2018;26:22750–60.
[233] Wang C, Wang L, Li X, et al. Few-layer bismuthene for femtosecond soliton molecules generation in Er-doped fiber laser. Nanotechnology 2018;30:025204.
[234] Ge Y, Chen S, Xu Y, et al. Few-layer selenium-doped black phosphorus: synthesis, nonlinear optical properties and ultrafast photonics applications. J Mater Chem C 2017;5:6129–35.
[235] Xie Z, Zhang F, Liang Z, et al. Revealing of the ultrafast third-order nonlinear optical response and enabled photonic application in two-dimensional tin sulfide. Photon Res 2019;7:494–502.
[236] Wu L, Xie Z, Lu L, et al. Few-layer tin sulfide: a promising black-phosphorus-analogue 2D material with exceptionally large nonlinear optical response, high stability, and applications in all-optical switching and wavelength conversion. Adv Opt Mater 2018;6:1700985.
[237] Huang W, Xie Z, Fan T, et al. Black-phosphorus-analogue tin monosulfide: an emerging optoelectronic two-dimensional material for high-performance photodetection with improved stability under ambient/harsh conditions. J Mater Chem C 2018;6:9582–93.
[238] Yao Y, Lin Z, Li Z, Song X, Moon KS, Wong CP. Large-scale production of two-dimensional nanosheets. J Mater Chem 2012;22:13494.
[239] Knieke C, Berger A, Voigt M, Taylor RNK, Röhrl J, Peukert W. Scalable production of graphene sheets by mechanical delamination. Carbon 2010;48:3196–204.
[240] Paton KR, Varrla E, Backes C, et al. Scalable production of large quantities of defect-free few-layer graphene by shear exfoliation in liquids. Nat Mater 2014;13:624–30.
[241] Woomer AH, Farnsworth TW, Hu J, Wells RA, Donley CL, Warren SC. Phosphorene: synthesis, scale-up, and quantitative optical spectroscopy. ACS Nano 2015;9:8869–84.
[242] Varrla E, Paton KR, Backes C, et al. Turbulence-assisted shear exfoliation of graphene using household detergent and a kitchen blender. Nanoscale 2014;6:11810–9.
[243] Varrla E, Backes C, Paton KR, et al. Large-scale production of size-controlled MoS_2 nanosheets by shear exfoliation. Chem Mater 2015;27:1129–39.
[244] Karagiannidis PG, Hodge SA, Lombardi L, et al. Microfluidization of graphite and formulation of graphene-based conductive inks. ACS Nano 2017;11:2742–55.